

Impact Response of Polymeric Train Sleepers

(For braskem company)

A draft version of reports is presented as completed activities

First part: lateral impact on polymeric material

Abstract

The impact response of railway sleepers made of high-density polyethylene and Glass Fiber Reinforced Polypropylene Compound was accessed via transverse impact tests using a drop hammer facility. The sleepers were subjected also to a wide range of temperatures, including extreme negative ones. The impact was properly monitored so information, like load profile, was accessed. The results can be used for finite element analyses purposes so the design of polymeric sleepers can be performed and improved as an alternative for traditional materials like wood and concrete.

1. Introduction

Railway sleepers keep the rail tracks in their position and transfer the train and cargo weight to the ballast bed [1,2]. The sleepers are traditionally being manufactured of timber, prestressed concrete, and steel. The wide variety of materials emphasizes that none of the above-mentioned materials is the best option, i.e besides their suitable advantages each has some disadvantages, thus the railway industry is seeking new materials to improve the railway transportation quality [3].

These days composite sleepers have emerged as the substitute for timber sleepers [4]. Composite materials offer several excellent properties such as high strength (stiffness) to weight ratios, good resistance against corrosion, moisture, and insects [3]. However, the application of composite sleepers is extremely limited [3–5]. The design and production cost of the composite parts has been the main barrier against the wide usage of composite materials in many industries like aerospace, automotive, and railway. However, developing reliable finite element codes and less expensive manufacturing processes is making composite material more competitive to the traditional materials, since today more than 50 % of the structural weight of new passenger airplanes like the Boeing 787 Dreamliner and Airbus A350 are made of composite materials. Thus composite sleepers also could gain more attention in the future.

Besides the price, composite sleepers are somewhat new with unknown *in-situ* and long-term performance [5], and their impact response strain rate sensitivity, and effect of different environment temperatures on mechanical properties of polymer composites sleepers have been less investigated yet.

A railway sleeper is likely to experience impact loading that lasts for a fraction of a second. The magnitude of the loads is very higher than quasi-static loads within a very short impulse duration (2–10 ms) [2] [3,6]. The effects of impact loads are critical issues in the design process of sleepers in railway systems. The wheel/rail abnormalities, such as wheel flat or dished rail, could produce impact loads that will transmit to the sleepers [5]. Moreover, a direct impact between wheels and sleepers during derailments [7] could produce significant impact loads and consequential damages to the sleepers.

A comprehensive review of studies that have considered dynamic impact loads in the railway system is provided in Ref [2]. The dynamic effects of rail/wheel abnormalities like rail corrugation, wheel flats, and shells, worn wheel and rail profiles, bad welds or joints, and track imperfections, are classified based on the time duration, magnitude, and shape of impact loads. It is concluded that the typical magnitude of the above-mentioned abnormalities is between 100 kN to 750 kN which is a function of train speed. The duration of these impact loads varies between 1 to 12 ms [2].

The drop hammer rigs have been widely utilized to investigate the impact response of railway sleepers [3,5,7–10]. The test set-ups are quite similar, a body mass so-called impactor with specific mass dropped from a height on the sleeper, to investigate derailment [7], or on the assembly of rail track and sleeper [5]. Based on available data in the literature, the average weight of the impactors is approximately 500 kg and the average drop height has been considered equal to 750 mm above the specimens (impact energy equal to 3.6 kJ). Most of the above-mentioned investigations have considered prestressed concrete sleepers under impact load.

The effect of reinforcing concrete sleepers with macro synthetic fiber under impact loading conditions was investigated using a drop hammer rig in Ref. [5]. The impactor having 52 kg mass was dropped from 1000 mm height on the rail track and prestressed concrete once. This impact scenario led to impact forces that lasted about 10 ms and had peak loads around 700 kN. A minimal effect of fibers on the impact force has been reported in this study. It is concluded that it is necessary to develop numerical models for impact simulation to understand the impact behavior of sleepers in a less expensive manner rather than experimental procedures.

Although several polymeric composite sleepers have been developed and utilized in several countries, impact test results on these relatively new sleepers are rarely available in the open literature [3]. For example, in Ref. [7] the impact results of the FFU synthetic sleeper, developed by Sekisui Chemical Co. Ltd. in Japan, are presented. In this study, a body with a mass of 500 kg and a cutting edge shaped like a wheel flange is dropped from a height of 75 cm twice for each test and lands on the edge of a sleeper inclined at 30° [7].

Finite element models of impact on the assembly of rail track and sleepers have been developed, for instance, the Ls-Dynal model of impact presented in Ref. [6]. However, experimental drop hammer tests are required to validate the finite element models.

The present study aims to investigate the impact response of a polymeric composite rail sleeper developed by Braskem company under different impact energies. Since it was observed that environment temperature will change the mechanical properties of the polymeric composite material of the sleeper, the effects of extremely low temperature on the impact response of the sleepers were investigated and compared to the results of impact tests at room temperature. The results could be useful to develop reliable FE models of polymeric sleepers under dynamic loadings.

2. Experimental impact test description

The impact investigation was conducted using a drop hammer test facility at the University of Sao Paulo, GMSIE laboratory, Fig. 1 shows the schematic presentation of the drop hammer rig. The impactor (striker) of the drop hammer has a maximum capacity of 1000 kg and 10-meter height above the anvil. The drop hammer test can be equipped with several measuring and imaging devices like high-speed cameras, laser velocimeter, accelerometers, and load cells.

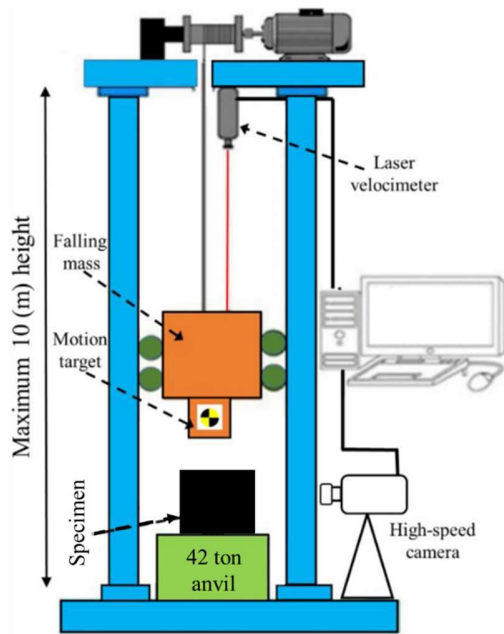
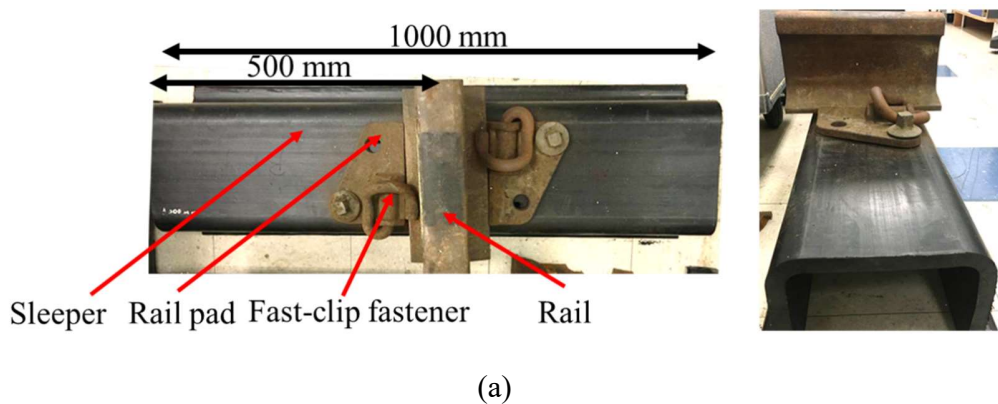
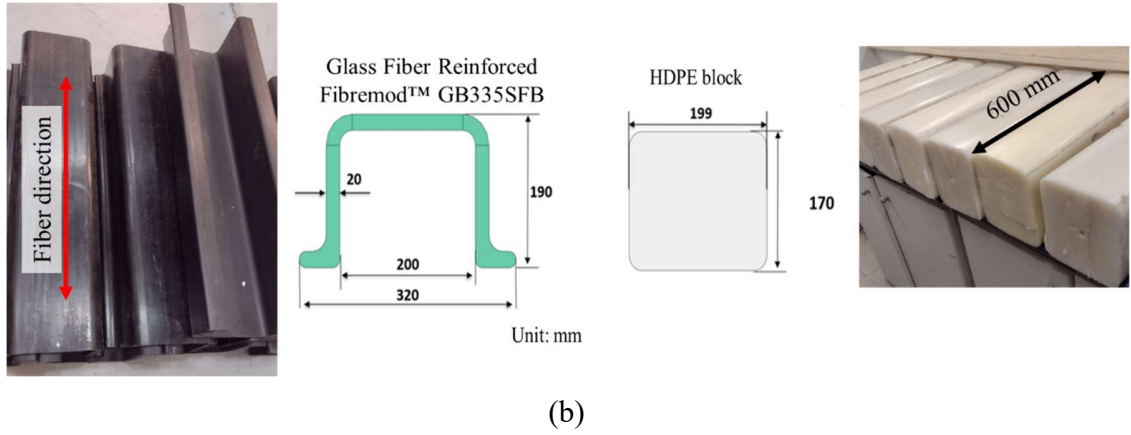


Fig. 1. Schematic of Drop hammer facility at GMSIE laboratory.

Impact tests were conducted on the assembly of rail, rail-pad, fast-clip fasteners, and composite sleeper, as illustrated in Fig. 2(a). The composite sleepers consist of two parts; (i) glass fiber-reinforced composite part (the U-shape) and (ii) block of HDPE, see Fig. 2(b). The length of the U-shape part is 1000 mm and the HDPE block having 600 mm length is placed in the middle of the U-shape part. However, before testing 150 mm of U-shape part's ends was trimmed to facilitate the handling of specimens and also due to the size of the thermal chamber.



(a)



(b)

Fig. 2. Assembly of railway track and composite sleeper; (a) The assembly of rail track and sleeper, (b) The sleeper's parts.

Fig. 3 shows the impact set-up that was equipped with high-speed cameras, LED illuminations, optic sensors. Two high-speed cameras were used to record the impact event. Fastcam SA5 high-speed camera with 230 kfps was used to track the motion target to find displacement, velocity, and acceleration of the impactor during impact event via digital image correlation. This recording speed (230kfps) is equivalent to a 230 kHz sampling rate that is quite enough for the present low-velocity impact study. A colorful high-speed camera with (3) three kfps was used to capture the whole impact event on the sleepers see fig.3.

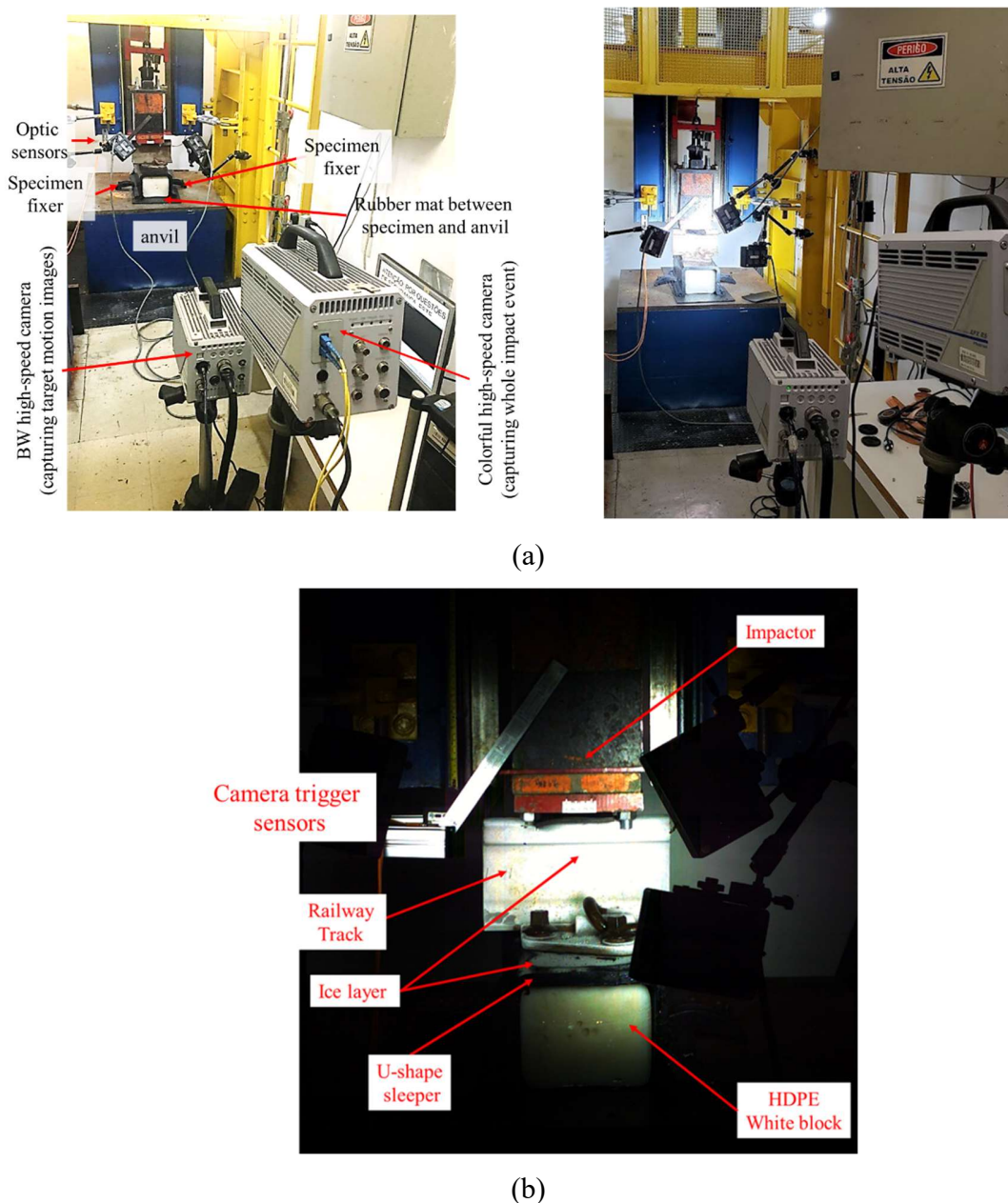


Fig. 3. Impact set-up; (a) General overview, (b) Zoom-in view of the real test.

The specimen was placed on the anvil of the drop hammer then it was positioned so that the impactor hits the rail track symmetrically. A soft rubber mat having 8 mm thickness, provided by Braskem, was placed between the sleepers and rigid face of the anvil (under sleeper pads (USP), as shown in Figs. 3 and 4.

The sleeper motion was restrained in some points to prevent any bounce back and tacking off the specimens from the anvil during the test [5]. Two clamps compress the edges of sleepers towards the anvil as shown in Fig. 4(a). Although these clamps restrict the vertical movement of the sleepers, however, most parts of the sleeper (U-shape part) could deform freely, Fig. 5 shows the deformation of the sleeper under impact.

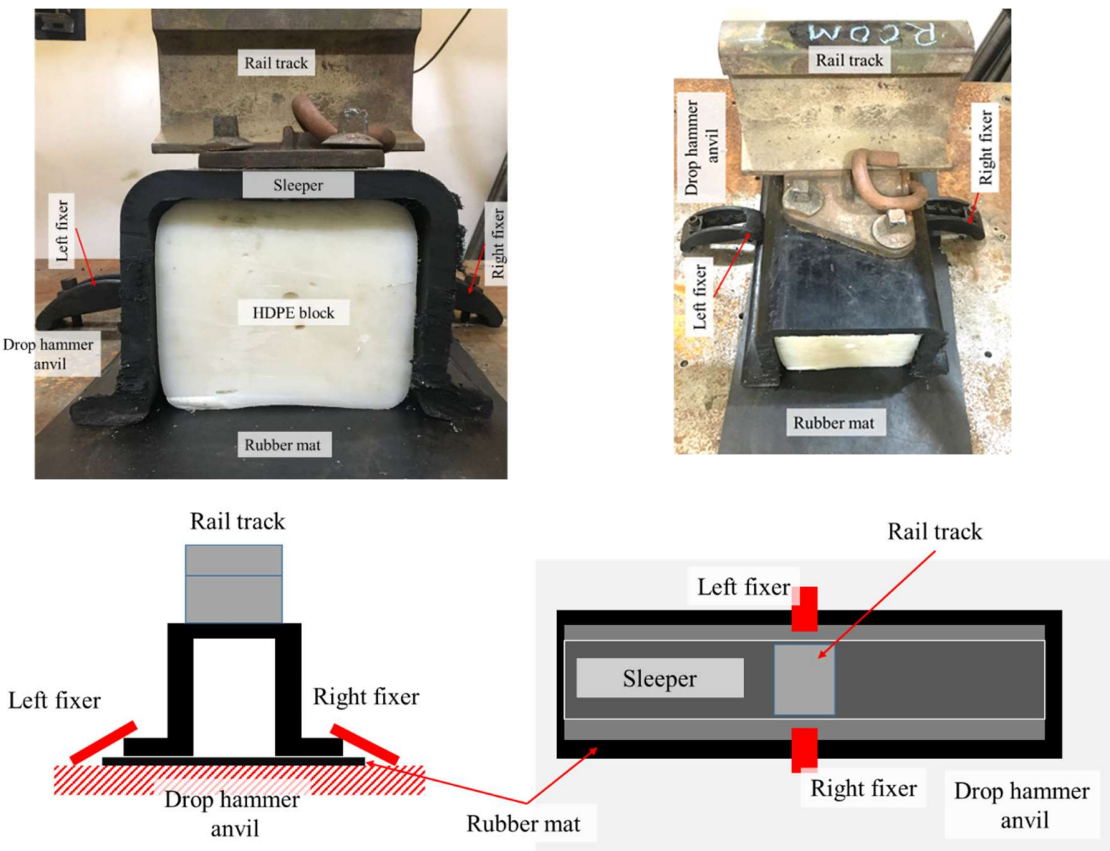


Fig. 4. Boundary condition of the sleeper.

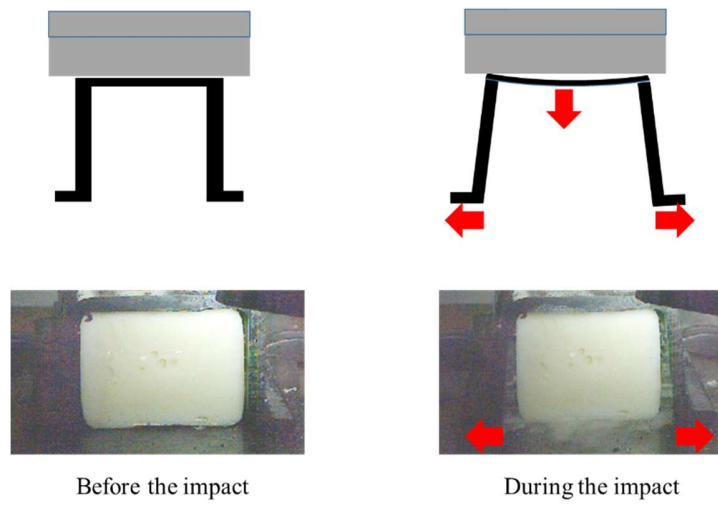


Fig. 5. Schematic and real presentations of deformation of sleeper under impact load.

Impact tests were conducted at room temperature ($\sim 25^{\circ}\text{C}$) and low temperature ($\sim -30^{\circ}\text{C}$). The assembly of the rail track and sleeper had been placed in a thermal chamber for a few hours to reach an acceptable thermal equilibrium. The specimens were placed in the thermal chamber where cold air was circulating over the specimen. Thermal chamber equipped with DC fans that blow air over buckets of dry ice (temperature of dry ice at surface is about -78°C). After a while, the air inside the thermal chamber reaches an extremely low and constant temperature. Then the specimen was kept for several more hours at this low temperature. Finite element analysis was used to find minimum exposure time to have approximately uniform low temperature in all parts of the specimens, see Appendix A for more information.

Gom correlation software was used to analyze high-speed camera images to find, displacement, velocity, and acceleration of the impactor in the vertical direction, Fig. 6 shows the target motion and digital image correlation software.

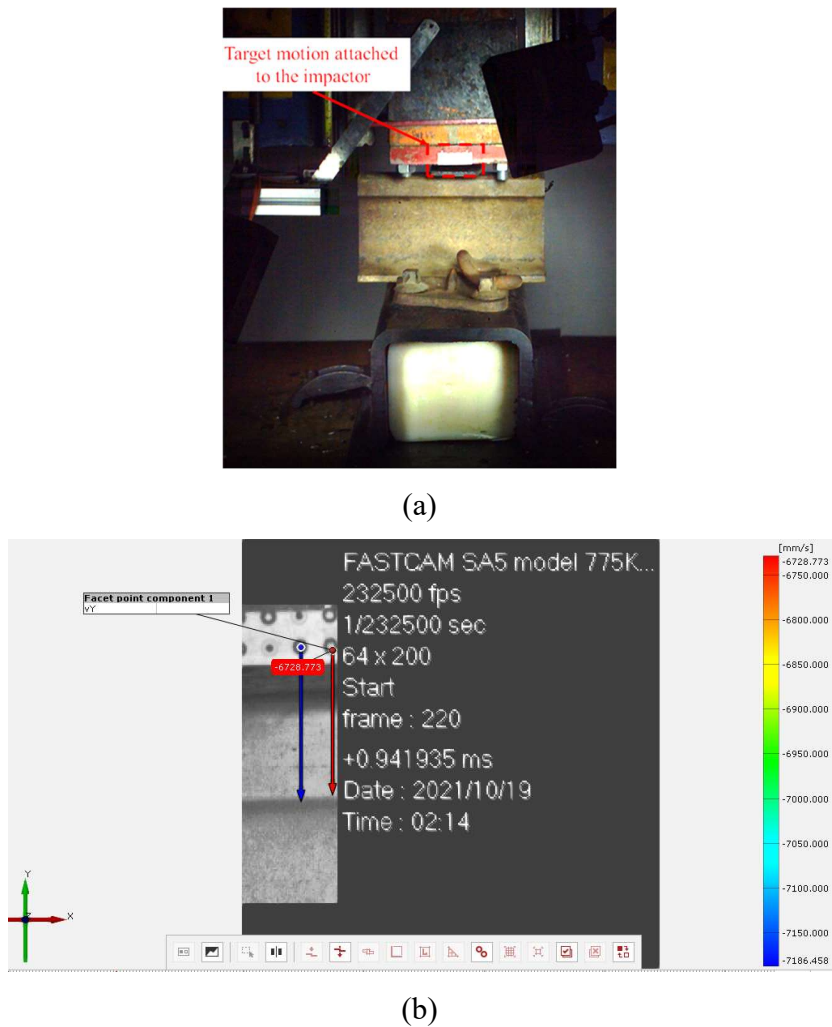


Fig. 6. Captured images with high-speed cameras during the impact test; (a) The target motion stickers, (b) Tracking motion target stickers using Gom correlation software.

The specimens were impacted with an impactor with constant mass (130 kg) and different initial velocities (different kinetic energies). The impactor is dropped repeatedly over the specimen and the height of the impactor increases after each impact for the next repeat. For each specimen testing procedure started with the lowest impact energy (impactor dropped from 1 (m) height above the specimens, impact energy equals 1.27 kJ), then after impact visual inspection was done to detect visible damage and failure. If no damage was detected the specimen was impacted again with higher kinetic energy. This procedure had been repeated until damage and failure were detected in the specimens. Fig. 7 shows the testing procedure.

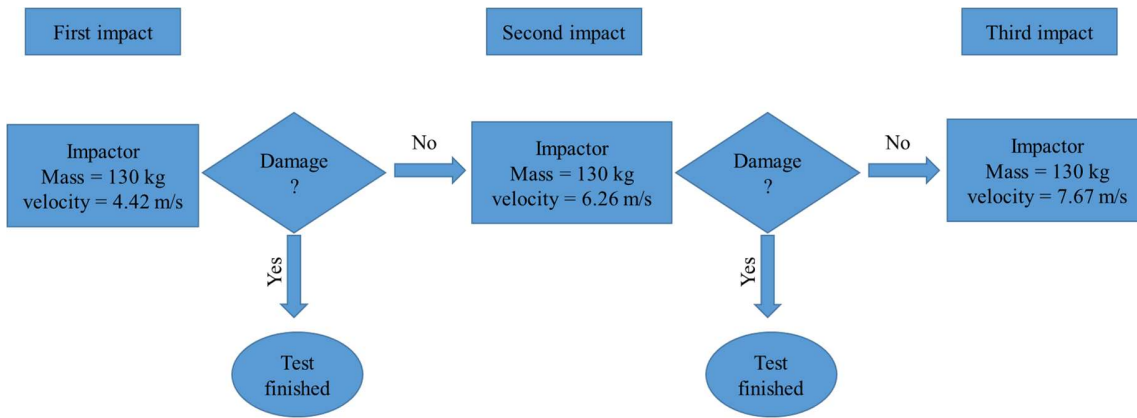


Fig. 7. Impact test procedure.

3. Results and discussion

The force-time histories of impact tests on the specimens are presented in this section. Moreover, the velocity and displacement of the impactor during impact tests were plotted against time.

A coding system to name the specimens under different conditions was conceived. The codes and definitions are listed in Table 1.

Table 1. Specimen coding system.

Specimen code	Testing condition	Drop height of the impactor (m)
IL1	Low temperature	1
IL2	Low temperature	2
IL3	Low temperature	3
IR1	Room temperature	1
IR3	Room temperature	3

3.1 Results of impact test on specimen IL1

The results of the impact test on the sleeper at low temperature while the impactor dropped from the lowest height, 1 (m) above the specimen, are presented in Fig. 8.

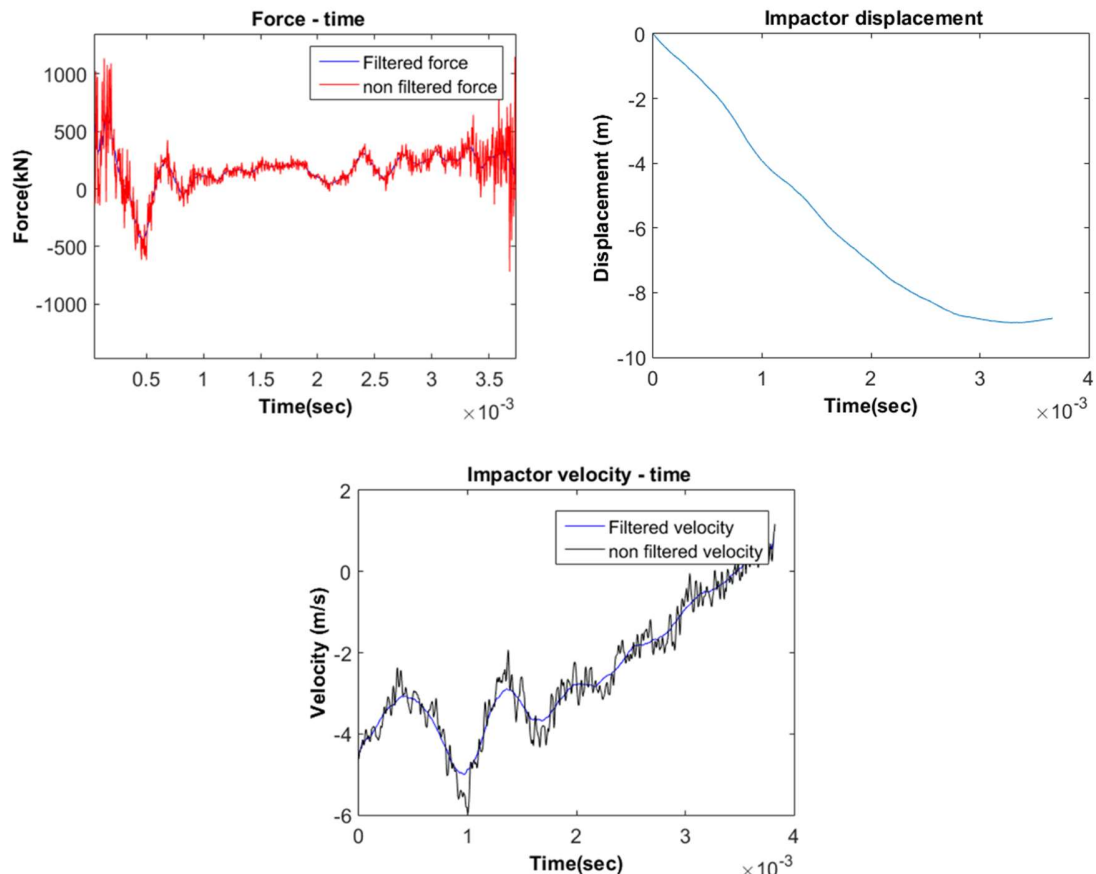


Fig. 8. Impact force on the specimen, displacement, and velocity of the impactor during the impact event; Specimen IL1.

Table 2 lists some features of the impact test on the IL1 specimen. It is worth noting that displacement of the impactor is equal to permanent, elastic deformation of the specimen and the rubber mat between the anvil and sleeper.

Table 2. Impact test results; Specimen IL1.

The maximum displacement of the impactor (mm)	8.8
Average force (kN)	168
Peak force (kN)	1000
Impact energy (kJ)	1.275
Visible damage	Not observed

3.2 Results of impact test on Specimen IL2

The results of the impact test on the sleeper at low temperature while the impactor dropped from 2 (m) height above the specimen are presented in Fig. 9.

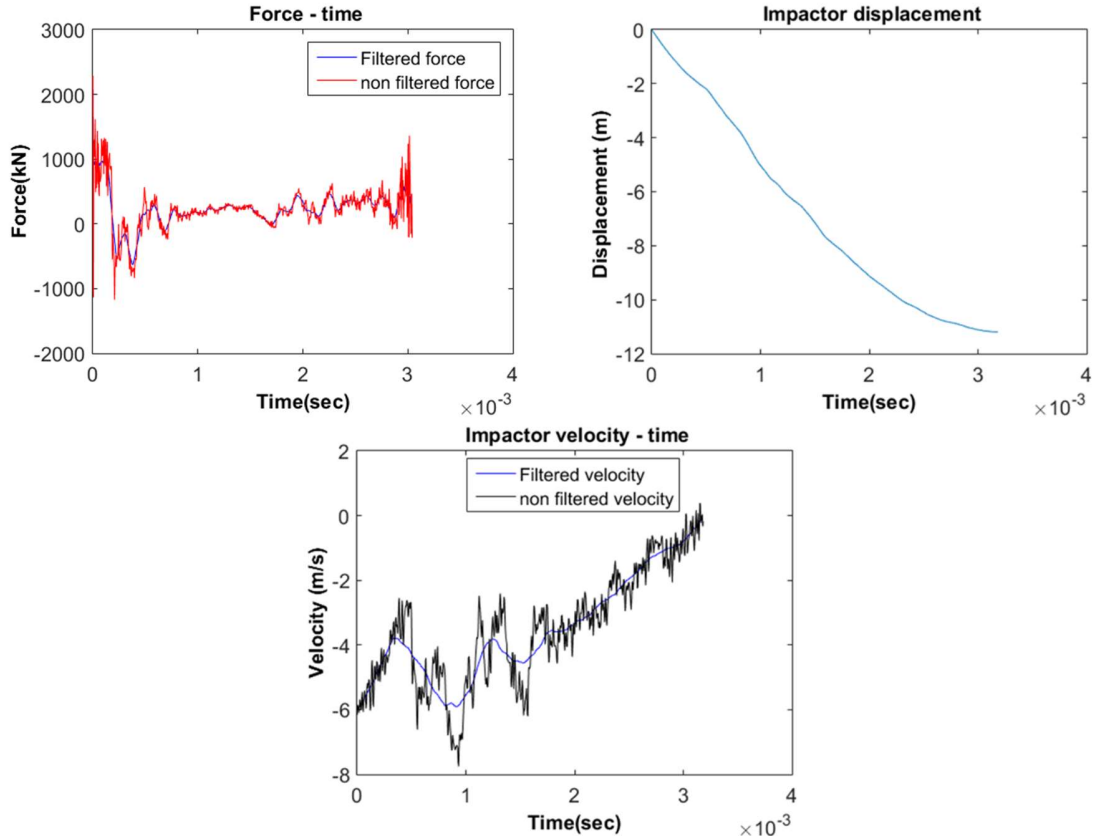


Fig. 9. Impact force on the specimen, displacement, and velocity of the impactor during the impact event; Specimen IL2.

Table 3 lists some features of the impact test on the IL2 specimen. It is worth noting that displacement of the impactor is equal to permanent, elastic deformation of the specimen and the rubber mat between the anvil and sleeper.

Table 3. Impact test results; Specimen IL2.

The maximum displacement of the impactor (mm)	10.9
Average force (kN)	230
Peak force (kN)	1701
Impact energy (kJ)	2.55
Visible damage	Not observed

3.3 Results of impact test on Specimen IL3

The results of the impact test on the sleeper at low temperature while the impactor dropped from 3 (m) height above the specimen are presented in Fig. 10.

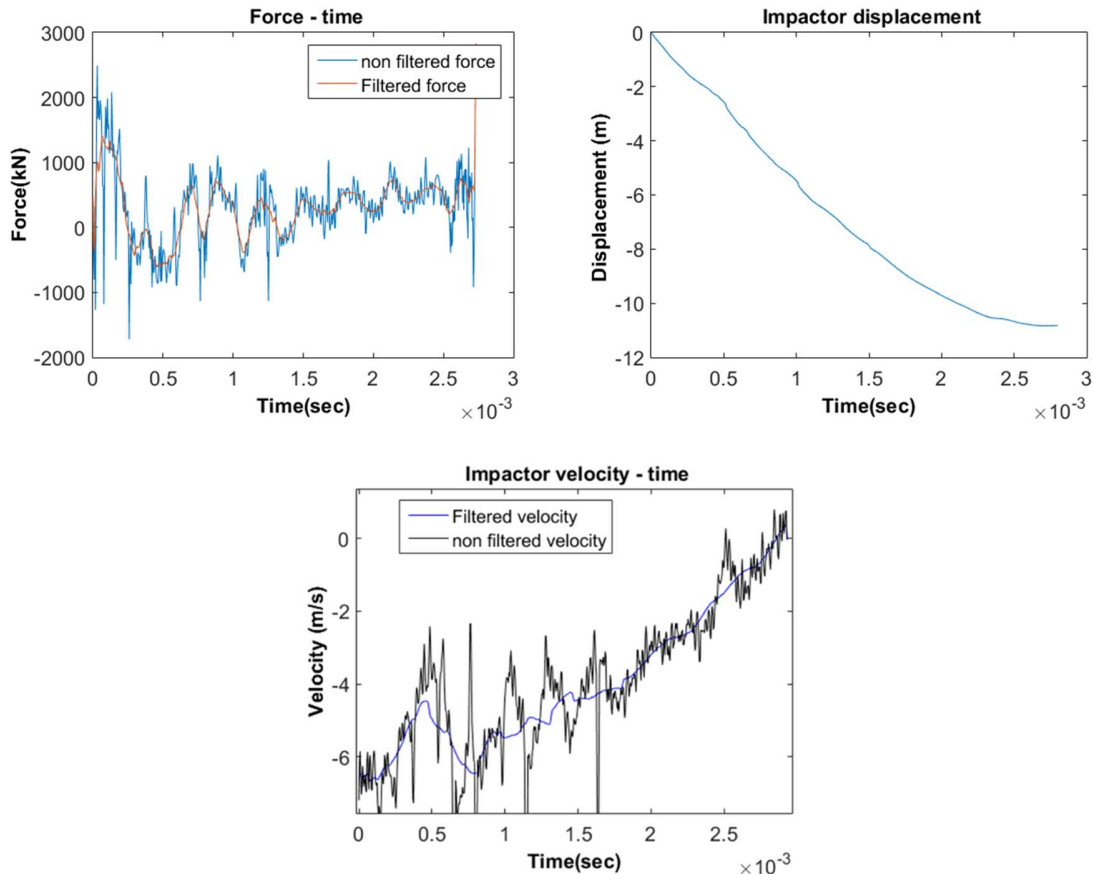


Fig. 10. Impact force on the specimen, displacement, and velocity of the impactor during the impact event; Test @ low-temperature and the impactor dropped from 3 (m) height above the specimen.

Table 4 lists some features of the impact test on the IL3 specimens. It is worth noting that displacement of the impactor is equal to permanent, elastic deformation of the specimen and the rubber mat between the anvil and sleeper.

Table 4. Impact test results; Specimen IL3.

The maximum displacement of the impactor (mm)	11.1
Average force (kN)	350
Peak force (kN)	1950
Impact energy (kJ)	3.82
Visible damage	Observed

For all specimens, post-impact visual inspection was conducted to detect any damage and failure in the sleepers. Fig. 11 shows the damages observed on the U-shaped part of the sleeper IL3 specimen (test @ low-temperature and the impactor dropped from 3 (m) height above the specimen).

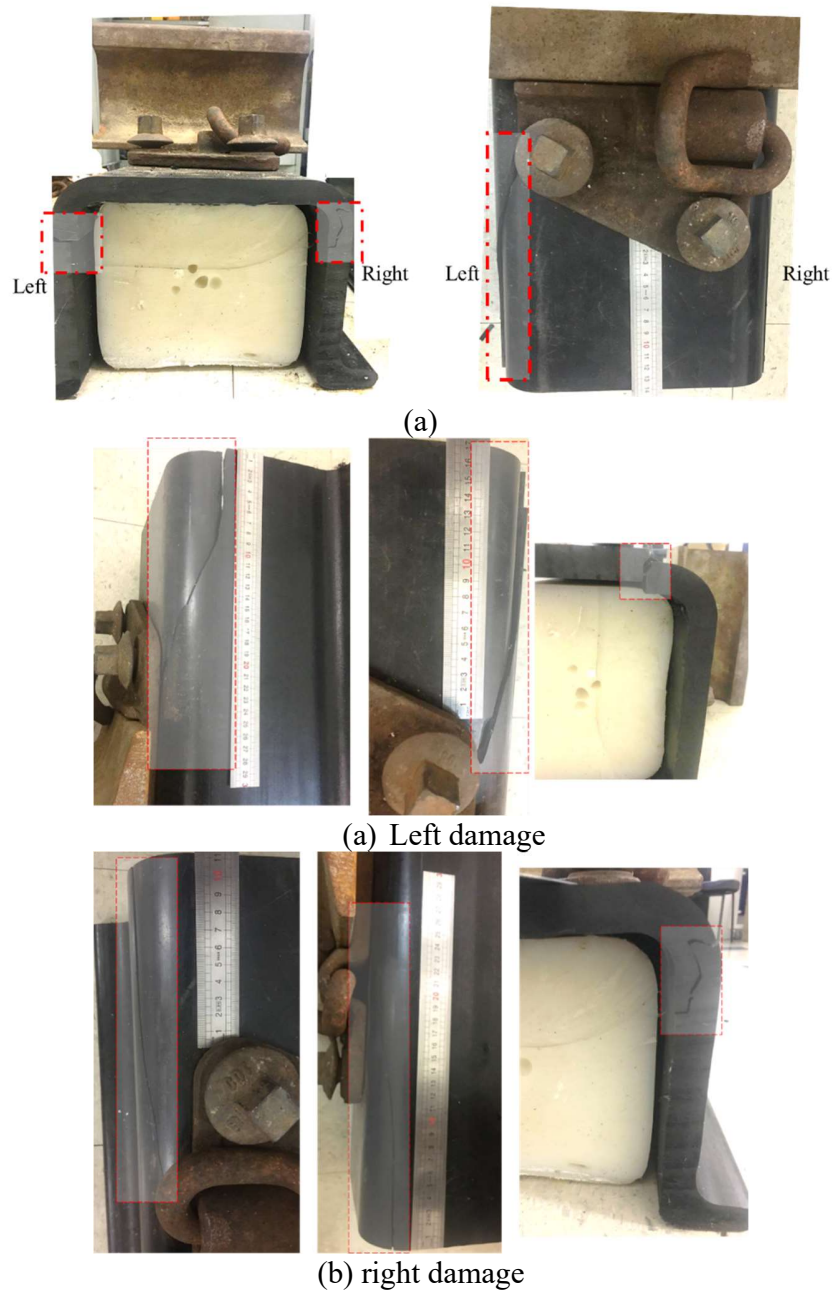


Fig. 11. Detected damage and failure in the sleeper after impact; Specimen IL3.

Figs. 12 and 13 show the damage initiation and propagation directions on the IL3 specimens. Crack on the left side initiated under the rail pad on the horizontal region of the U-shape sleeper. Then the crack developed on the vertical side of the sleeper and ended up on the end of the sleeper (see Fig. 12(a) and Fig. 13). Both cracks on the right and left of the sleeper developed only in one direction to the end of the sleeper, however, the right side crack initiated on the vertical side (end of the sleeper) and developed to the center of the sleeper. The crack on the right side did not reach the horizontal part of the sleeper (see Fig. 12(b)).

The crack on the left was initiated due to the high-stress condition under the rail and rail pad, however, the crack on the right was initiated due to large deformation of the vertical side of the sleeper.

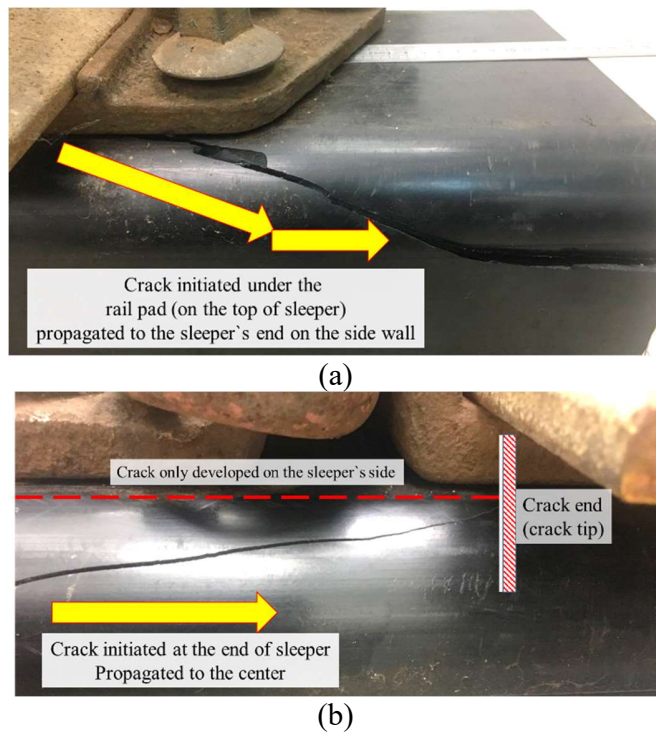


Fig. 12. Crack location, initiation, and propagation on the U-shaped sleeper part; (a) Left side, (b) Right side; Specimen IL3.

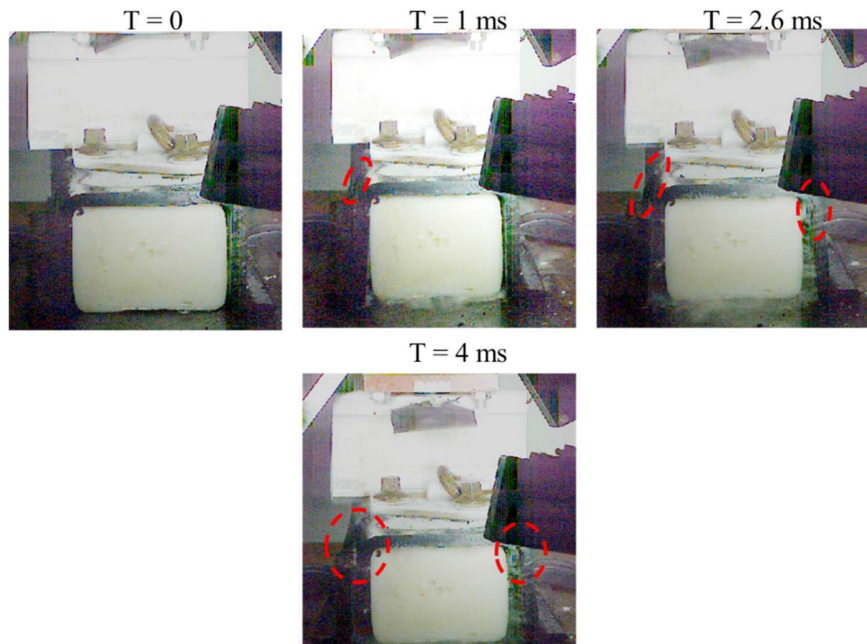


Fig. 13. Deformation and damaging of sleeper under impact load; Specimen IL3.

3.4 Results of impact test on Specimen IR1

The results of the impact test on the sleeper at room temperature while the impactor dropped from the lowest height, 1 (m) above the specimen, are presented in Fig. 14.

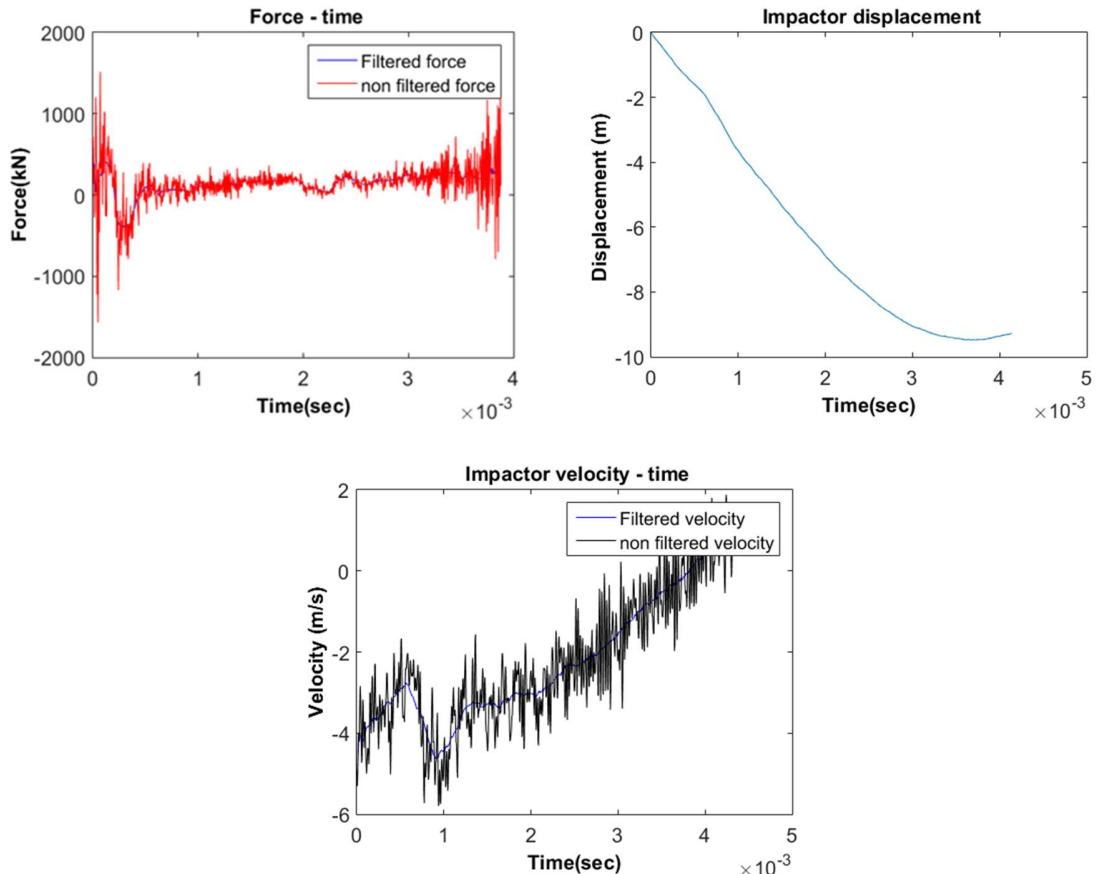


Fig. 14. Impact force on the specimen, displacement, and velocity of the impactor during the impact event; Specimen IR1.

Table 5 lists some features of the impact test on the IR1 specimens. It is worth noting that displacement of the impactor is equal to permanent, elastic deformation of the specimen and the rubber mat between the anvil and sleeper.

Table 5. Impact test results; Specimen IR1.

The maximum displacement of the impactor (mm)	9.6
Average force (kN)	167.91
Peak force (kN)	920
Impact energy (kJ)	1.275
Visible damage	Not observed

3.5 Results of impact test on Specimen IR3¹

Fig. 15 shows the results of the impact on sleeper at room temperature while impactor was released from 3 (m) height above the specimen.

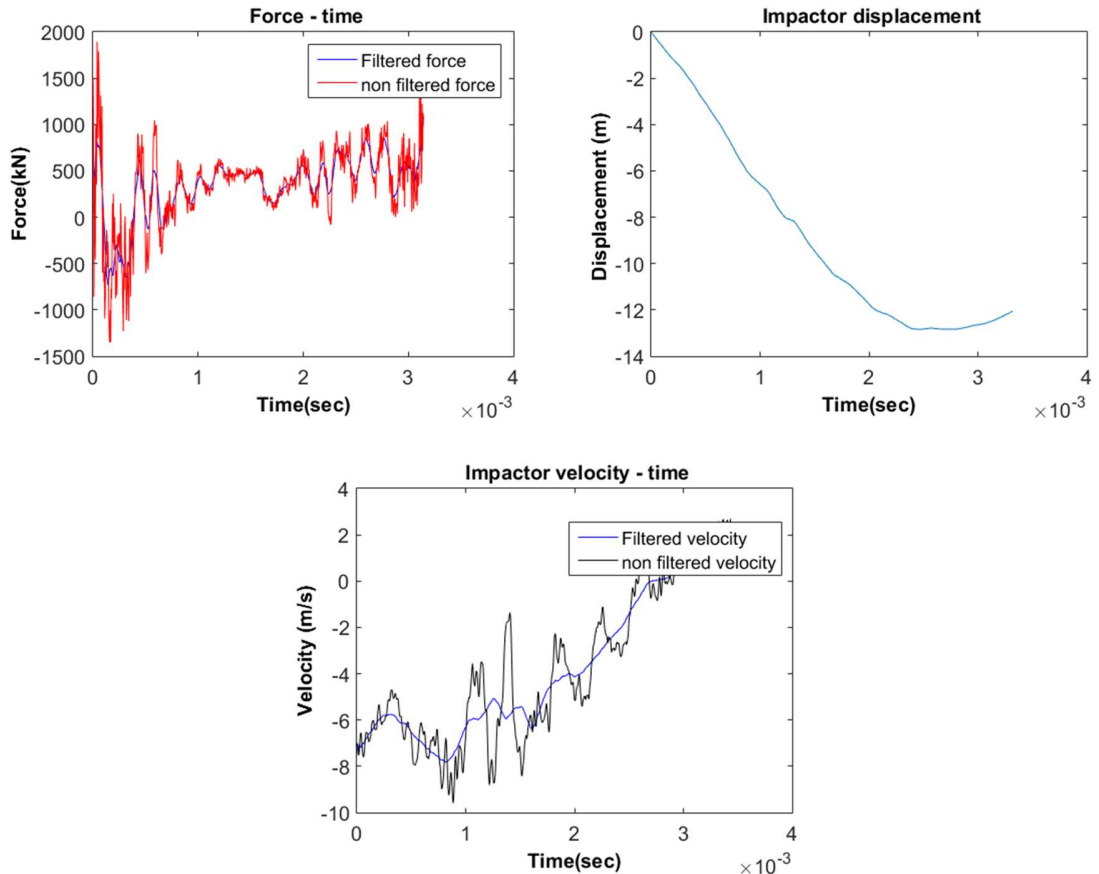


Fig. 15. Force and velocity of impactor during the impact event; Specimen IR3.

Table 6 lists some features of the impact test on the IR3 specimens. It is worth noting that displacement of the impactor is equal to permanent, elastic deformation of the specimen and the rubber mat between the anvil and sleeper.

Table 6. Impact test results; Specimen IR3.

The maximum displacement of the impactor (mm)	12.1
Average force (kN)	361
Peak force (kN)	1860
Impact energy kJ	3.82
Visible damage	Not observed

¹ Since the specimen IL2 (low temperature and 2 (m) drop height) did not fail, thus test on the specimen IR2 (room temperature and 2 m (m) drop height) is ignored and test on IR3 conducted after IR1 test.

For both IR1 and IR3 specimens, post-impact visual inspection was conducted however, no visible damage was detected

The boundary condition of specimen IR3 is different from the BC of the other specimens in this study. For the IR3 specimen, the left fixer is placed in the middle of the sleeper (under the rail track similar to the other specimens), however, the right fixer is placed in the front of the sleeper. This modification was inevitable since due to the high impact energy of the previous test (IL3) the fixture hole on the anvil was extremely damaged.

3.6 Comparison between specimens

The typical impact force history for all specimens (assembly of the rail and sleeper) can be divided into 3 stages; in the first stage impact force increase rapidly and reach its maximum value, then the impact force decreases dramatically (Stage II). During the third stage, the impact force oscillates around the average force. The typical impact force on the specimens is presented in Fig. 16.

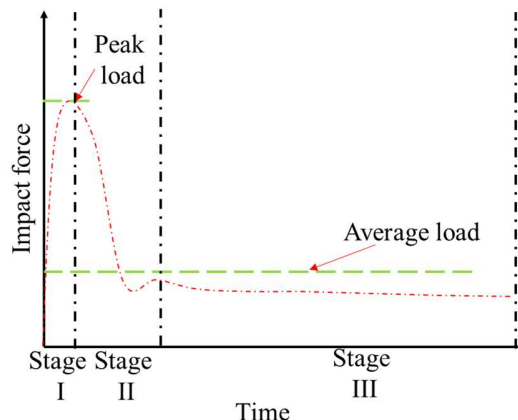


Fig. 16. Typical impact force history of all specimens in this study.

3.6.1 Effect of temperature on the impact behavior of the specimens

Fig. 17 compares the maximum deformation of vertical sides of the U-shape part of IR3 and IL3 specimens. Since both specimens were impacted by the same kinetic energy,

low temperature could be the main reason that the IL3 specimen failed under impact loading².



Fig. 17.Temperature effect on the deformation of specimens under the highest impact energy in this study.

In contrast to obvious damages on the IL3 specimen, it seems that low temperature did not have a significant effect on the impact forces of IR3 and IL3 specimens as shown in Fig. 18 (a). this issue could emphasize that the main load-bearing part of the sleepers is the HDPE block. Comparison between impact forces of IR1 and IL1 specimens shows that low temperature caused an increase in the peak load, however, the values of impact forces at the third stage are approximately the same for IR1 and IL1 specimens (Fig. 22(b)).

² Both HDPE (white block) and Fibremod™ GB335SFB (U-shape part) material become more brittle at lower temperature.

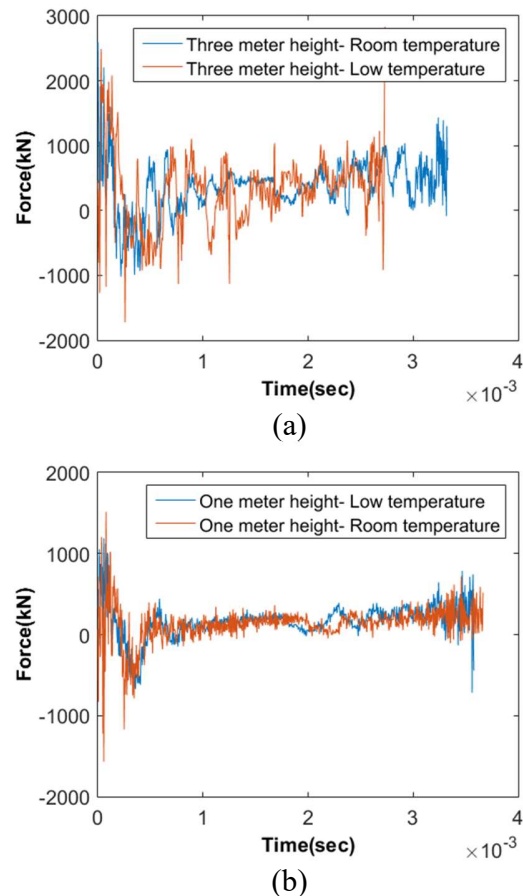


Fig. 18. Effect of temperature on the impact forces; (a) comparison between IR3 and IL3 specimens, (b) Comparison between IR1 and IL1 specimens.

3.6.2 Effect of impact energy on the impact response of the specimens

The effect of impact energy on the impact forces is presented in Fig. 19. In general, with an increase in impact energy both peak load and average impact force are increased.

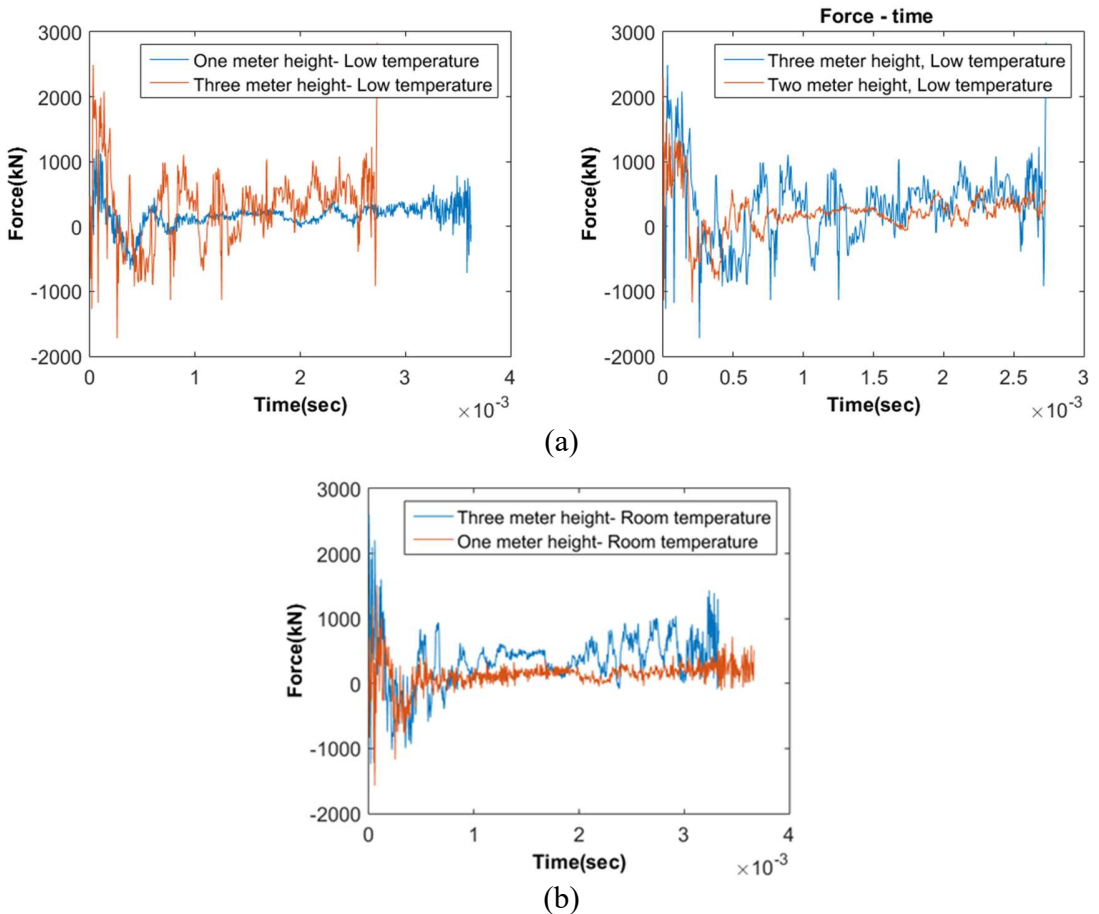


Fig. 19. The effect of impact energy on the impact force on the specimens; (a) Comparison between IL1 and IL3 specimens and IL2 and IL3 specimens, (b) Comparison IR1 and IR3 specimens.

The increase in kinetic energy led to the higher impact force and larger instability (deformation) of vertical sides of the U-shape sleeper as depicted in Figs. 20 and 21. The IL3 specimen failed due to damages on the U-shape part, as depicted in Figs. 11-13. However, the impact force of IL3 has not experienced a significant decrease and is recorded higher than the impact forces of IL1 and LI2 specimens. In the word the block of HDPE is the main load-bearing component, thus even after the failure of the U-shape part the impact force capacity of the sleeper (assembly of U-shaped and with HDPE block) remained high for the IL3 specimen.

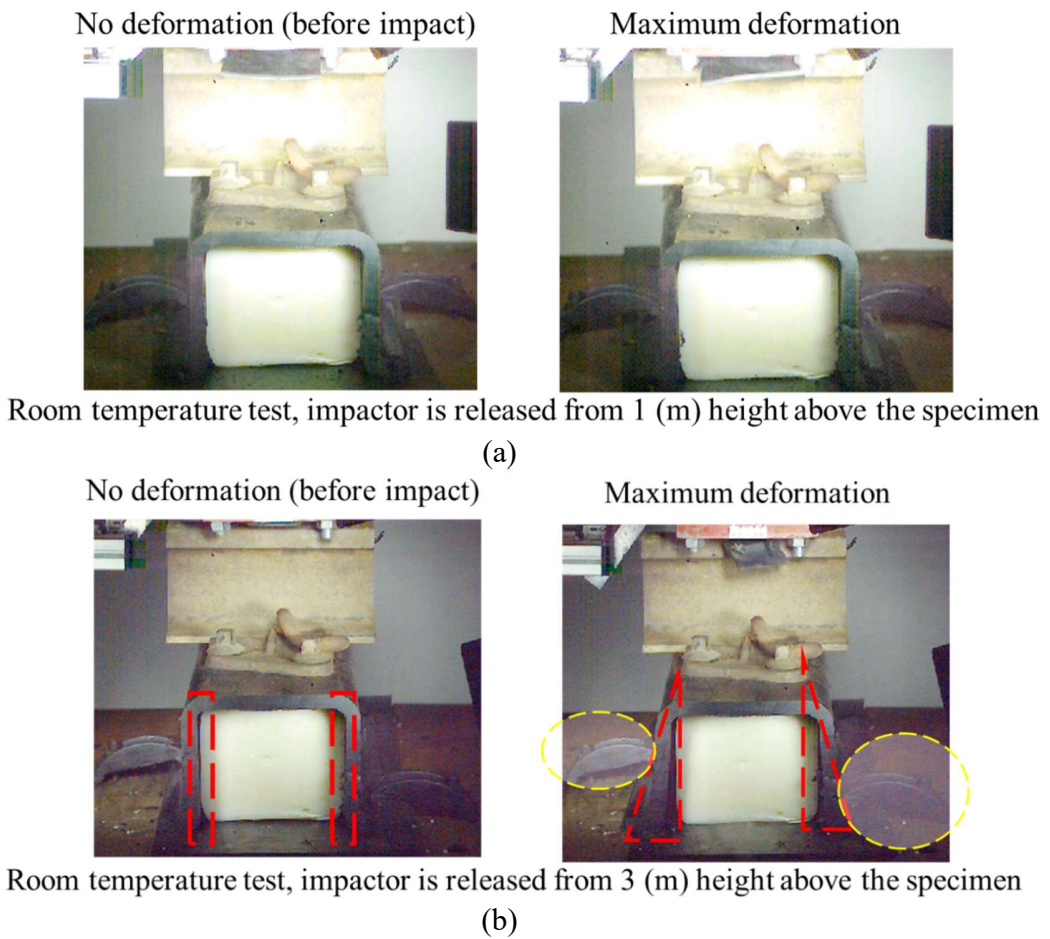


Fig. 20. Effect of impact energy on deformation of sleepers; (a) Specimen IR1, (b) Specimen IR3.

The U-shape part of the sleepers distributes the load over a larger area of the HDPE block and may have no direct significant contribution to the compressive load-bearing capacity of the whole sleeper. Under compressive impact force, the vertical sides of the U-shape part became unstable (Figs. 13, 20, 21), even the HDPE block could act similar to a wedge and facilitate the instability of the U-shape part. The area near the corners of the U-shape part underwent large deformations, thus it is likely that failure occurs in these regions. However, the boundary condition in the present study is applied only to prevent the specimens from taking off from the anvil and it could be completely different from their real boundary condition in the field.

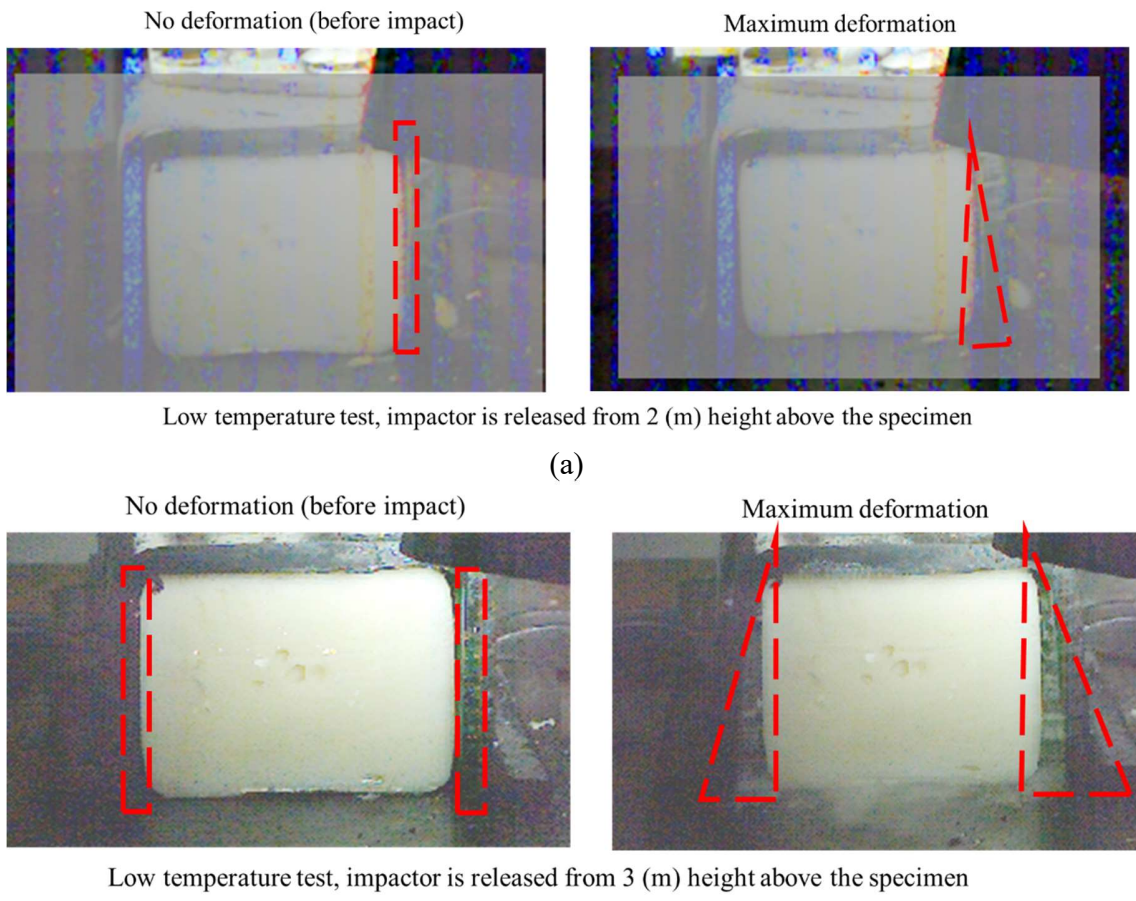
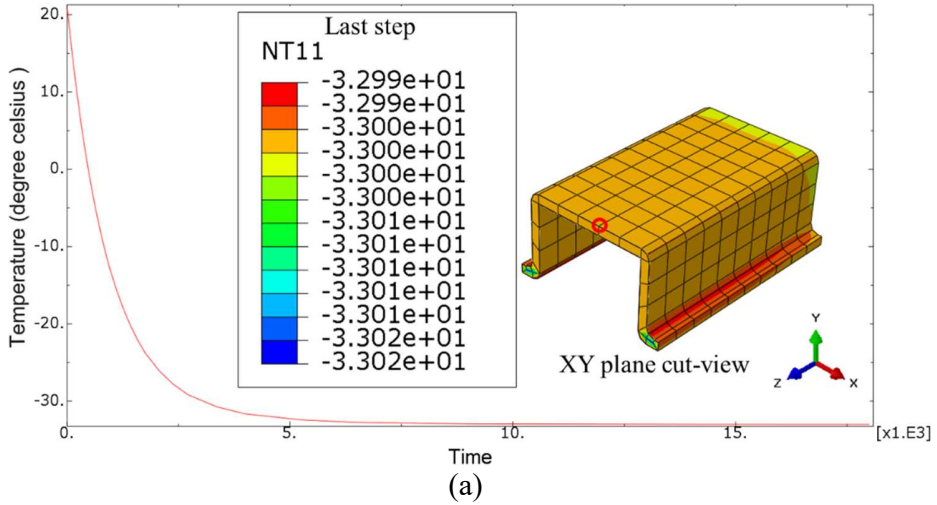


Fig. 21. Effect of impact energy on deformation of sleepers; (a) Specimen IL2, (b) Specimen IL3.

4. Conclusions

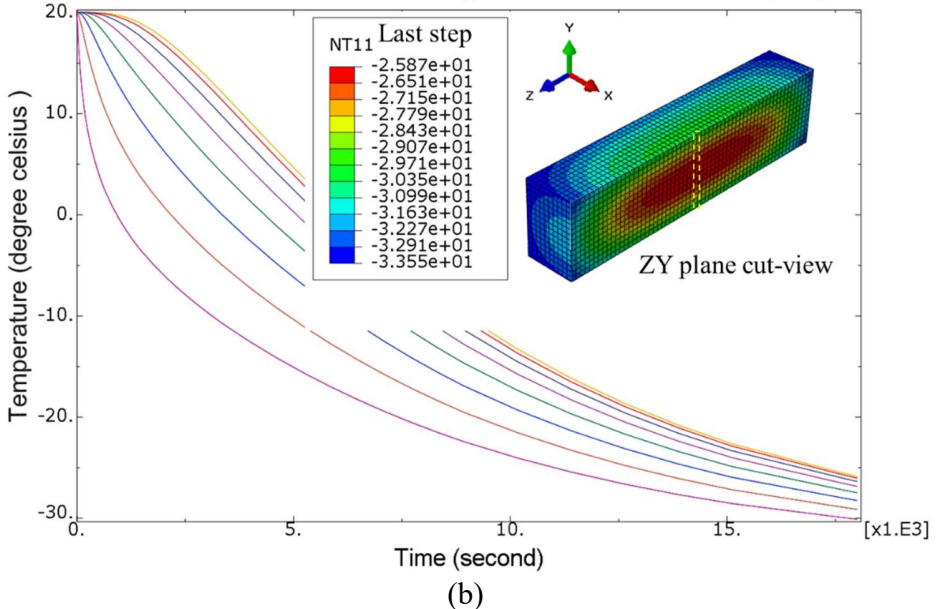
Appendix A: Thermal finite element analysis

Fig. A1 shows the nodal temperature for the HDPE block and U-shape Fibremod GB335SFB part after five hours. Table A1. List the thermal properties in the FE model.



(a)

Note: The plotted line shows nodal temperature values at the highlighted node.



(b)

Note: The plotted lines show nodal temperature values at highlighted nodes.

Fig. A1. FE results for thermal analysis (cooling down) of sleeper's parts; (a) U-shape part, (b) HDPE block.

During the experiments, the assembly of rail track, rail pad, fast clip, fasteners, sleeper, and HDPE block, was placed in the thermal chamber. After sealing the chamber and running DC fans, it lasted around 60 minutes that air temperature inside the chamber reached

to -28 to -31. Then the assembly was kept in the chamber for approximately 270 additional minutes before removing from the chamber and positioning under the drop hammer.

Table A1. Thermal properties were selected for both materials.

Thermal properties	Value
Specific heat ($\text{J}\cdot\text{kg}^{-1}\cdot\text{K}^{-1}$)	1400*
Conductivity ($\text{W}/(\text{m}\cdot\text{K})$)	0.5*
Density (kg/m^3)	940 (HDPE) 1180 (Fibremod GB335SFB)**

** Braskem

* Assumed based on values available in the literature.

References

- [1] A. Raj, P. Nagarajan, A.P. Shashikala, Failure prediction of impact behaviour of self-compacted rubcrete sleepers, *Mater. Des. Process. Commun.* 3 (2021). doi:10.1002/mdp2.174.
- [2] A.M. Remennikov, S. Kaewunruen, A review of loading conditions for railway track structures due to train and track vertical interaction, *Struct. Control Heal. Monit.* 15 (2008) 207–234. doi:10.1002/stc.227.
- [3] W. Ferdous, A. Manalo, G. Van Erp, T. Aravinthan, S. Kaewunruen, A. Remennikov, Composite railway sleepers – Recent developments, challenges and future prospects, *Compos. Struct.* 134 (2015) 158–168. doi:10.1016/j.compstruct.2015.08.058.
- [4] G. VAN ERP, M. MCKAY, Recent Australian Developments in Fibre Composite Railway Sleepers, *Electron. J. Struct. Eng.* 13 (2013) 62–66. <https://ejsei.com/EJSE/article/view/161>.
- [5] C. Camille, D. Kahagala Hewage, O. Mirza, T. Clarke, Full-scale static and single impact testing of prestressed concrete sleepers reinforced with macro synthetic fibres, *Transp. Eng.* 7 (2022) 100104. doi:10.1016/j.treng.2022.100104.
- [6] C. Ngamkhanong, S. Kaewunruen, Effects of under sleeper pads on dynamic responses of railway prestressed concrete sleepers subjected to high intensity impact loads, *Eng. Struct.* 214 (2020) 110604. doi:10.1016/j.engstruct.2020.110604.
- [7] G. Koller, FFU synthetic sleeper – Projects in Europe, *Constr. Build. Mater.* 92 (2015) 43–50. doi:10.1016/j.conbuildmat.2015.03.118.
- [8] S. Kaewunruen, A.M. Remennikov, Experiments into impact behaviour of railway prestressed concrete sleepers, *Eng. Fail. Anal.* 18 (2011) 2305–2315. doi:10.1016/j.englfailanal.2011.08.007.
- [9] A.S. Hameed, A.P. Shashikala, Suitability of rubber concrete for railway sleepers, *Perspect. Sci.* 8 (2016) 32–35. doi:10.1016/j.pisc.2016.01.011.

- [10] R. V Dukkipati, R. Dong, Impact Loads due to Wheel Flats and Shells, *Veh. Syst. Dyn.* 31 (1999) 1–22. doi:10.1076/vesd.31.1.1.2097.

Second part

Static and dynamic material characterization at different temperature conditions

A draft version of the final report is presented here

1. Material system

This report presents the quasi-static material characterization of two materials; (I) High-Density Polyethylene (HDPE) GD5150K and (II) Polypropylene (PP) Compound, Glass Fiber Reinforced, Fibremod™ GB335SFB. These two materials are provided by the client in the form of components, blocks of GD5150K, and U-shape sleepers made of Fibremod™ GB335SFB, as illustrated in Fig. 1.



Fig. 1. Components that specimens were cut from; (a) GD5150K (white blocks), (b) Fibremod™ GB335SFB (black U-shape sleepers).

2. Tensile tests

Specimens are cut from the components presented in Fig. 1. Specimens are designed based on ASTM D638 ‘Standard Test Method for Tensile Properties of Plastics’ recommendations as presented in Fig. 2.

Note: In the present report ‘White material’ is used to refer to GD5150K material and ‘Black material’ is used to refer to GB335SFB material.

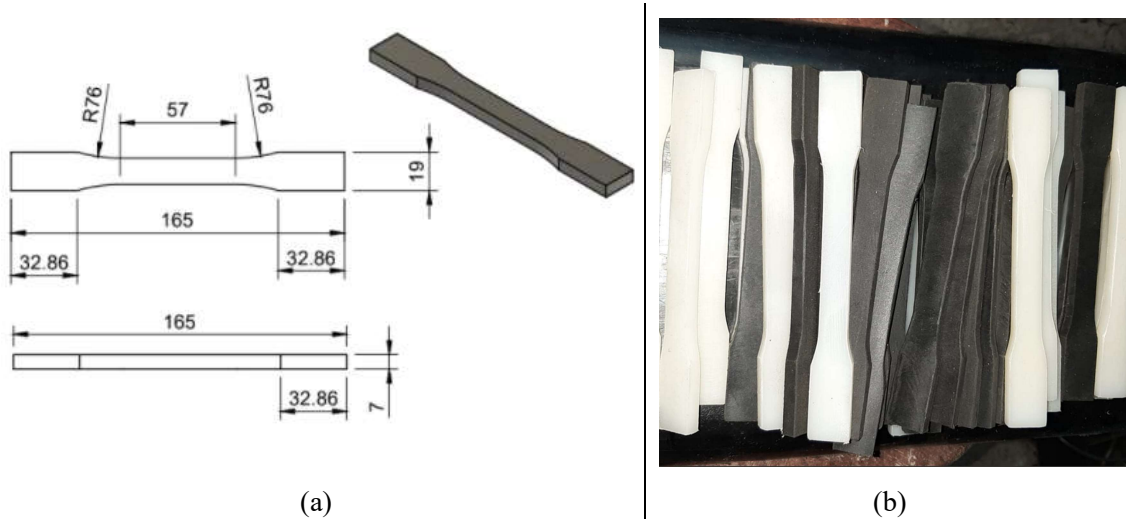


Fig. 2. Tensile test specimens design based on ASTM D638; (a) specimens' drawing, dimensions are in ‘mm’, (b) Extracted specimens form the components.

2.1 Tensile testing conditions

Instron 3369 machine is used to conduct Quasi-static tensile tests at two different crosshead velocities; (I): 1 mm/min (~ 0.05 in/min), and (II) 1 mm/s. Tests were conducted at three different temperatures; (I) Room temperature (21°C to 26°C), (II) Hot temperature ($\sim 50^\circ\text{C}$), and (III) Cold temperature ($\sim -17^\circ\text{C}$). The cold (hot) temperature was achieved by blowing cold (hot) air inside the chambers shown in Fig. 3.

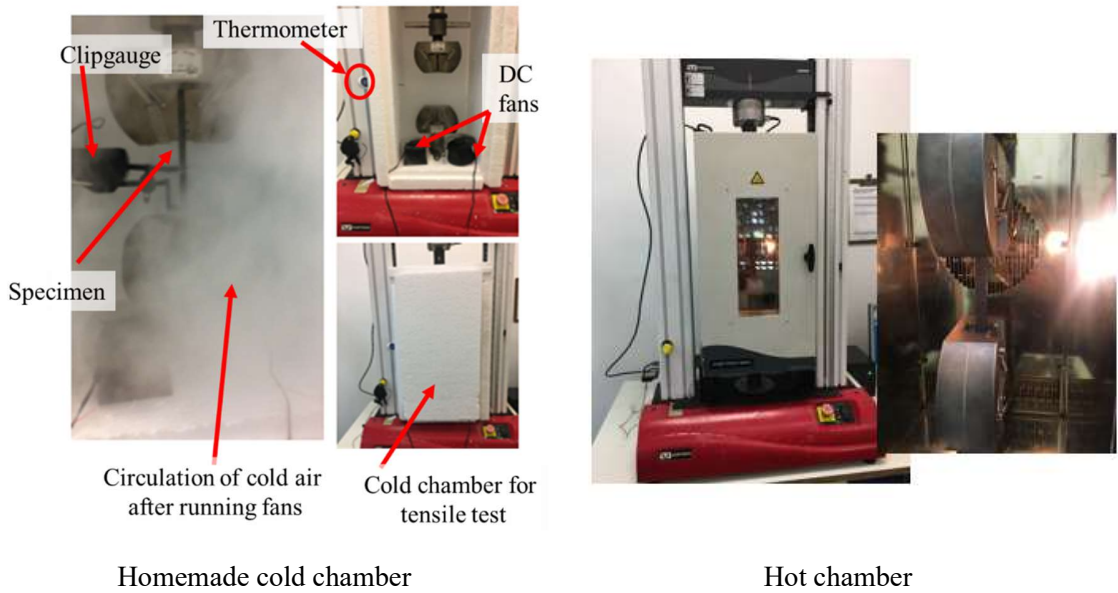


Fig. 3. Cold and hot chambers.

2.2 Specimens name abbreviation description

In contrast to GD5150K (white material), Fibremod™ GB335SFB (black material) has anisotropic behavior. Since material behavior in different directions is different, specimens of black material are cut from the sleepers in two orthogonal directions concerning the sleepers' centerline; these two directions are presented in Fig. 4.

Table 1 lists the names and their definitions that are used to refer to the materials and testing conditions in this report.

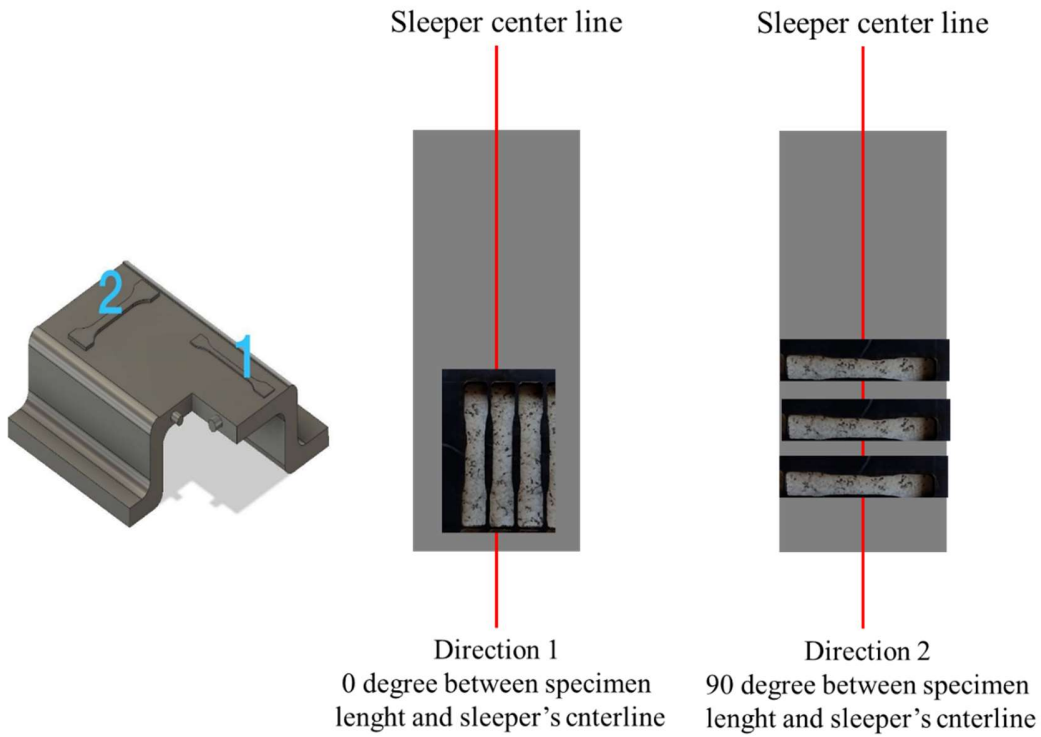


Fig. 4. The orthogonal directions that tensile specimens are cut from the black material (Fibremod™ GB335SFB).

Table 1. Description of tensile specimens reference names.

Specimen	Description
TB00C	T: Tensile test, B: Black material, 00: Angle between specimens length and sleeper's length, C: Cold temperature
TB00R	T: Tensile test, B: Black material, 00: Angle between specimens length and sleeper's length, R: Room temperature
TB00H	T: Tensile test, B: Black material, 00: Angle between specimens length and sleeper's length, H: Hot temperature
TB90C	T: Tensile test, B: Black material, 90: Angle between specimens length and sleeper's length, C: Cold temperature
TB90R	T: Tensile test, B: Black material, 90: Angle between specimens length and sleeper's length, R: Room temperature
TB90H	T: Tensile test, B: Black material, 90: Angle between specimens length and sleeper's length, H: Hot temperature
TWC	T: Tensile test, W: White material, C: Cold temperature
TWR	T: Tensile test, W: White material, R: Room temperature
TWH	T: Tensile test, W: White material, H: Hot temperature

2.3 tensile test results

2.3.1 Tensile results for TB90 specimens: black material (Fibremod™ GB335SFB), specimens are perpendicular to the sleeper's centerline

Fig. 5 illustrates the tensile behavior of TB90 specimens. Both temperature and loading rate changed the mechanical properties of TB90 specimens as was expected; however, the effect of temperature is more significant. Higher velocity and lower temperature decreased the material ductility. Table 2 lists the tensile properties of CB90 specimens under different testing conditions.

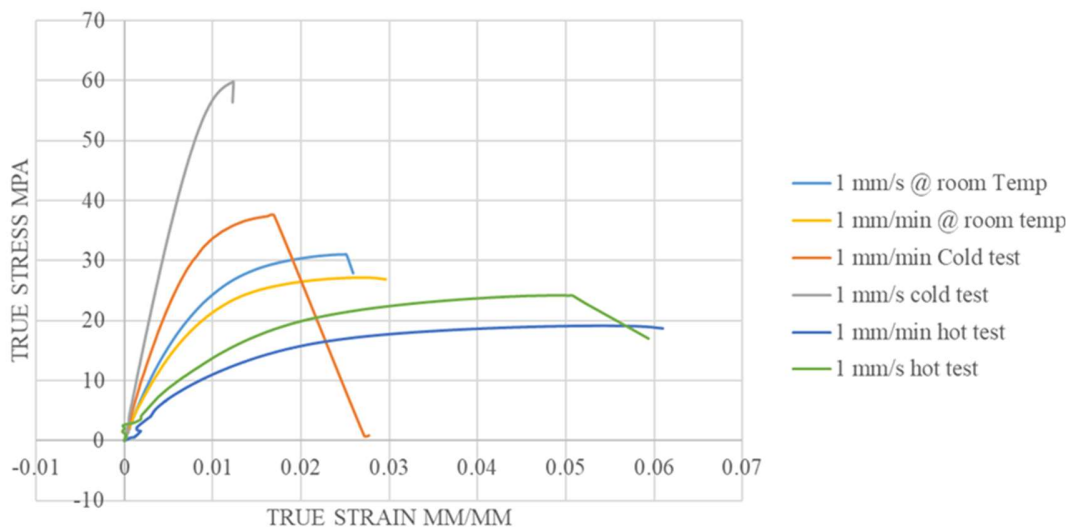


Fig. 5. True stress- true strain curves for TB90 specimens.

Table 2. Quasi-static tensile test TB90.

Test number	Elastic modulus (Mpa)	Failure ³ stress (Mpa)	Failure strain (mm/mm)	Yield stress (Mpa)	Strain @ yield point (mm/mm)
TB90R#1 1mm/s	3788±5%	30.23±1%	0.025	20.64±1%	0.007
TB90R#2 1mm/s	3738±5%	30.4±1%	0.028	21.79±1%	0.0078
TB90R #1 1 mm/min	3533±5%	25.6±1%	0.026	16±1%	0.0065

³ Rupture

TB90R #2 1 mm/min	3504±5%	26.1±1%	0.03	17.02±1%	0.006
TB90H #1 1 mm/min	1718±5%	17.5±1%	0.063	9.39±1%	0.00745
TB90H #2 1 mm/min	1215±5%	19±1%	0.056	12±1%	0.008
TB90H #1 1 mm/s	1426±5%	24.64±1%	0.041	16±1%	0.008
TB90H #2 1 mm/s	1481±5%	22±1%	0.052	15±1%	-
TB90C #1 1mm/min	5295±5%	33±1%	0.016	24±1%	0.0066
TB90C #2 1 mm/min	5039±5%	36±1%	0.017	30±1%	0.008
TB90C #1 1 mm/s	7491±5%	59±1%	0.012	53±1%	0.00918

2.3.2 Tensile results for TB00 specimens: Black material (Fibremod™ GB335SFB), specimens are parallel to the sleeper's centerline

Fig. 6 and Table 3 present the tensile behavior of black material in a 00-degree direction (parallel to the sleeper's centerline). illustrates the tensile behavior of TB90 specimens. Both temperature and loading rate changed the mechanical properties of TB90 specimens; however, the effect of temperature is more significant.

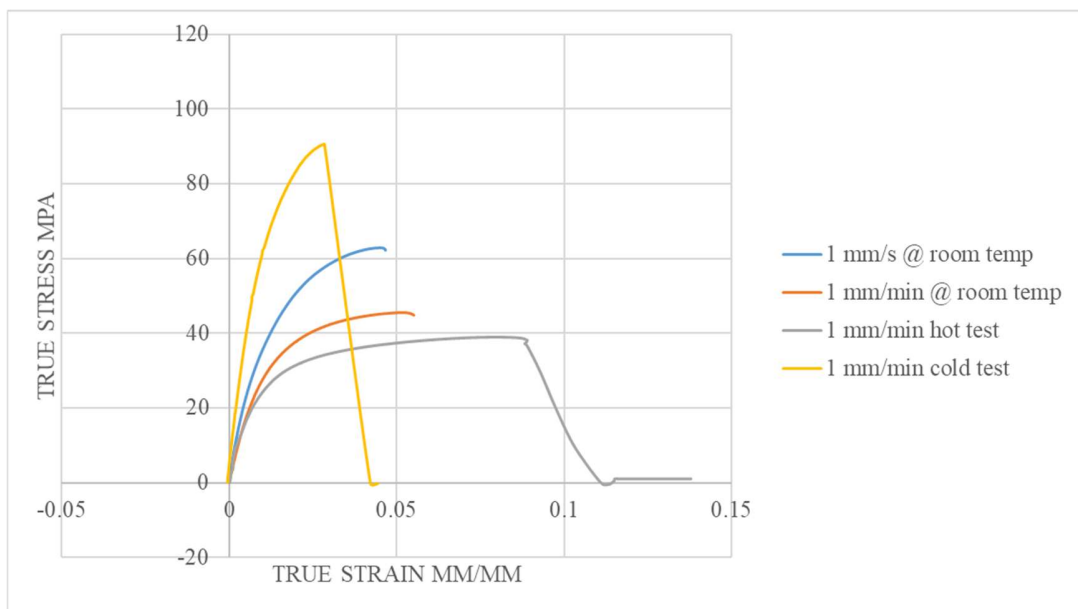


Fig. 6. True stress- true strain curves for TB00 specimens.

Table 3. Quasi-static tensile test TB00.

Test number	Elastic modulus (Mpa)	Failure ⁴ stress (Mpa)	Failure strain (mm/mm)	Yield stress (Mpa)	Strain @ yield point (mm/mm)
TB00R #1 1 mm/min	4700±5%	44±1%	0.055	20±1%	0.0063
TB00R #2 1 mm/min	4717±5%	48.47±1%	0.057	24.13±1%	0.0071
TB00R #1 1 mm/s	5361±5%	62±1%	0.046	29.93±1%	0.0076
TB00H#1 1 mm/min	3465±5%	39±1%	0.102	16±1%	0.006
TB00C #1 1 mm/min	9580±5%	90±1%	0.028	51.9±1%	0.007
TB00C #2 1 mm/min	10290±5%	94±1%	0.021	57±1%	0.007

⁴ Rupture

2.3.3 Tensile results for white material (GD5150K) TW specimens

True-stress – true strain curves for white material (TW specimens) under different testing conditions are presented in Fig. 7. Note: Fig. 7. Does not show the rupture point for the hot test (hot tests were stopped before the rupture occurs). Table \$ lists the tensile test results for TW specimens in detail.

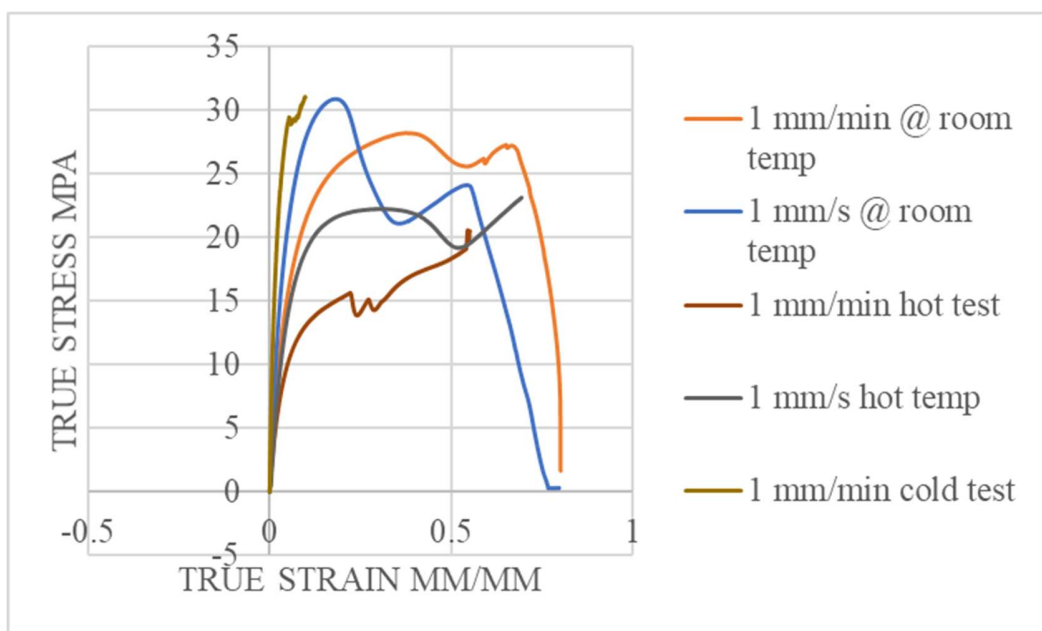


Fig. 7. True stress- true strain curves for TW specimens.

Table 4. Quasi-static tensile test TW.

Test number	Elastic modulus (Mpa)	Failure stress (Mpa)	Maximum achieved strain (mm/mm) ⁵	Yield stress (Mpa)	Strain @ yield point (mm/mm)
TWR#1 1 mm/min	503	-	<i>Eng</i> = 1.2 <i>True</i> = 0.8	8.22	0.018
TWR #2 1 mm/min	415	-	<i>Eng</i> = 0.97 <i>True</i> = 0.65	7.78	0.021

⁵ Since in some tests for TW specimens the crosshead of the Instron machine reached the environment chamber, maximum strain is not necessarily equal to strain @ rapture.

TWR #1 1 mm/s	691	-	0.98	9	0.015
TWR #2 1 mm/s	717	-	0.74	10.5	0.016
TWH #1 1 mm/min	314	-	0.7	7.54	0.029
TWH #1 1 mm/s	478	-	0.68	8.24	0.019
TWH #2 1 mm/s	450	-	0.69	6.00	0.022
TWC #1 1 mm/min	1841	31	0.30	11	0.008
TWC #1 1 mm/s	2926	24	0.35	25	0.0107
TWC #2 1 mm/s	-	29	0.37	20	0.012



Fig. 8. The TB00 and TB90 specimens after the tensile test.

2.4 Post tensile test inspection

Although loading rate and temperature have a significant effect on the tensile behavior of black and white materials, the visual inspection does not observe a remarkable change in the failure morphologies especially for black material as shown in Fig. 8. Fracture in TB90 specimens occurred in a uniform (flat) cross-section; however, the fractured cross-sections of TB00 specimens are not flat and uniform as observed in TB90 specimens, see Fig. 8.

In contrast to black material, the temperature had a significant effect on the elongation of TW (white material) specimens, see Fig. 9.

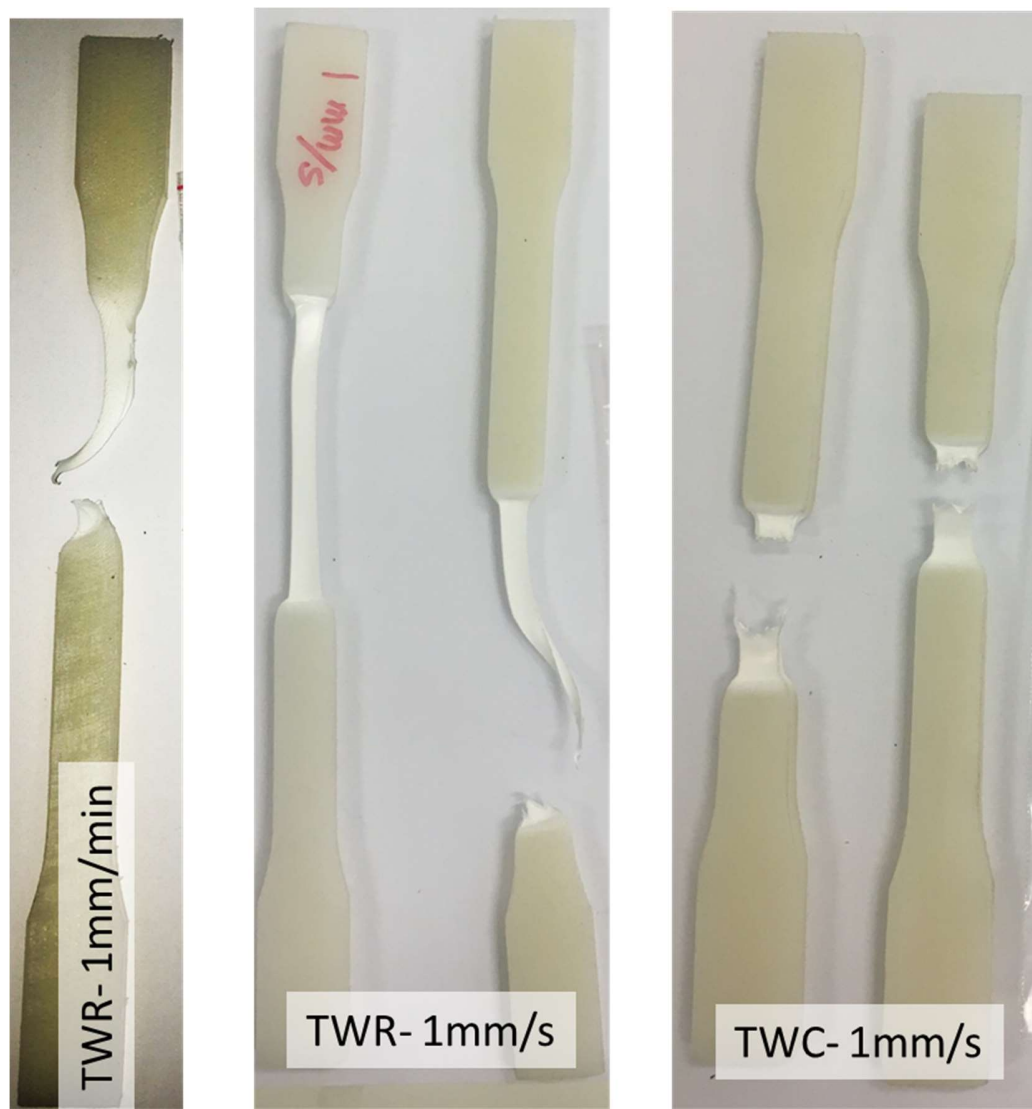


Fig. 9. The TW specimens after the tensile test.

3. Compression tests

Similar to tensile specimens, compression specimens were cut from components made of GD5150K (white blocks) and Fibremod™ GB335SFB (black U-shape sleepers). Specimens are designed based on D695 ‘Standard Test Method for Compressive Properties of Rigid Plastics’ recommendations as presented in Fig. 10. Note: the definitions of ’00-direction’ and ’90- direction’ for compression specimens made of black material are similar to that explained previously for tensile specimens, see Fig. 4.

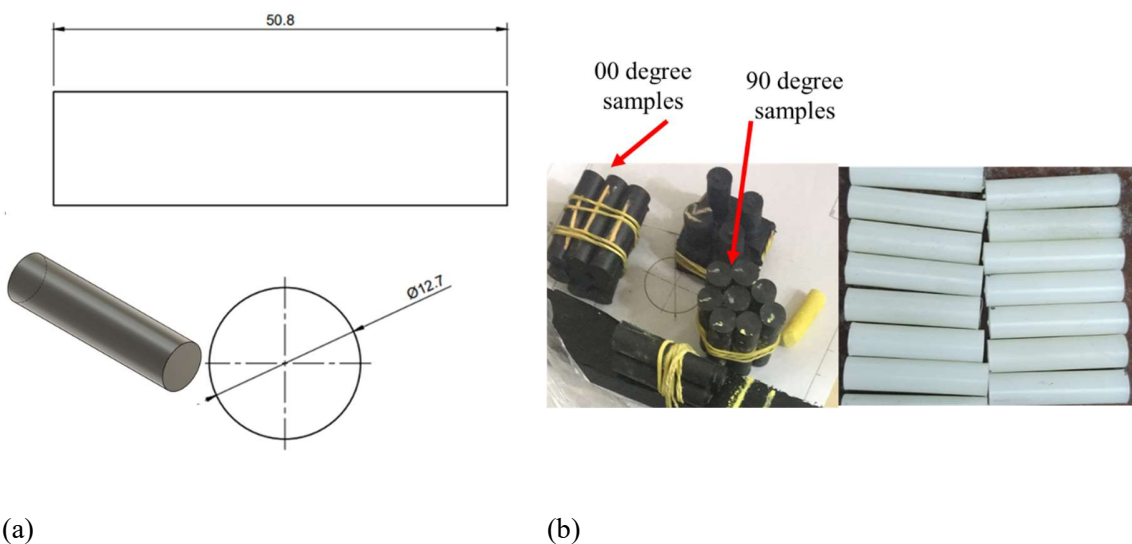


Fig. 10. Compression test specimens design based on ASTM D695; (a) Specimens’ drawing, dimensions are in ‘mm’; (b) Extracted specimens from the components.

3.1 Compression testing conditions

Testing machine Instron 3369 is used to conduct Quasi-static compression tests at two different crosshead velocities; (I): 1 mm/min and (II) 1 mm/s. Tests were conducted at three different temperatures; (I) Room temperature (21°C to 26°C), (II) Hot temperature (~ 50°C) using an Instron environment chamber, and (III) Cold temperature (~ -32°C) using a homemade cold chamber, see Fig 11.

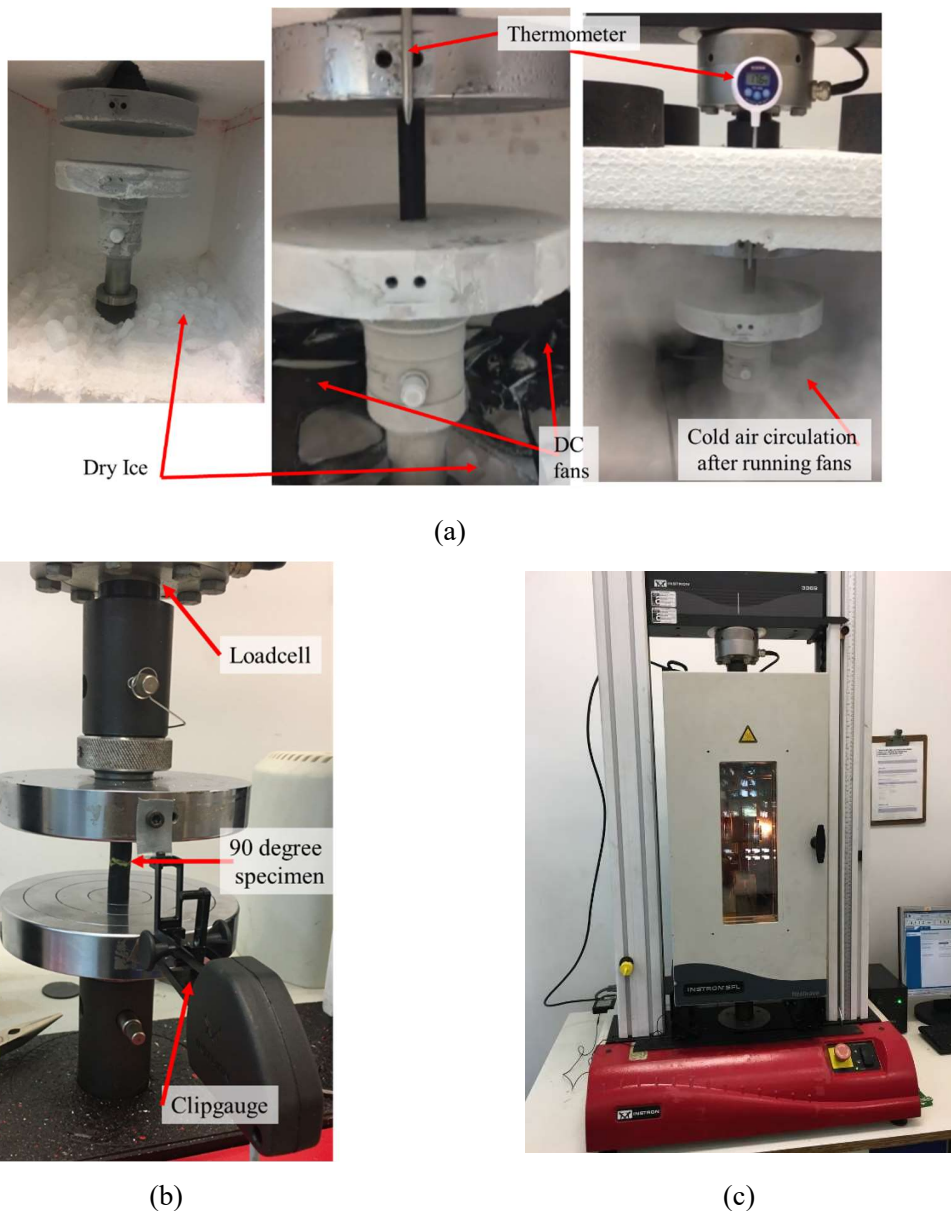


Fig. 11. Compression test setups.

Specimens reference names and their descriptions are presented in Table 5.

Table 5. Description of compression specimens' reference names.

Specimen	Description
CB00C	C: Compression test, B: Black material, 00: Angle between specimens length and sleeper's length, C: Cold temperature
CB00R	C: Compression test, B: Black material, 00: Angle between specimens length and sleeper's length, R: Room temperature

CB00H	C: Compression test, B: Black material, 00: Angle between specimens length and sleeper's length, H: Hot temperature
CB90C	C: Compression test, B: Black material, 90: Angle between specimens length and sleeper's length, C: Cold temperature
CB90R	C: Compression test, B: Black material, 90: Angle between specimens length and sleeper's length, R: Room temperature
CB90H	C: Compression test, B: Black material, 90: Angle between specimens length and sleeper's length, H: Hot temperature
CWC	C: Compression test, W: White material, C: Cold temperature
CWR	C: Compression test, W: White material, R: Room temperature
CWH	C: Compression test, W: White material, H: Hot temperature

3.2 Compression tests results

3.2.1 Compression test results for CB90: Test on black material (Fibremod™ GB335SFB), specimens are perpendicular to the sleeper's centerline

Fig. 12 shows results of CB90 specimens under quasi-static compressing load and different temperatures. Elastic modulus, yield stress, and strain @ yield point are presented in Table 6 for CB90 specimens.

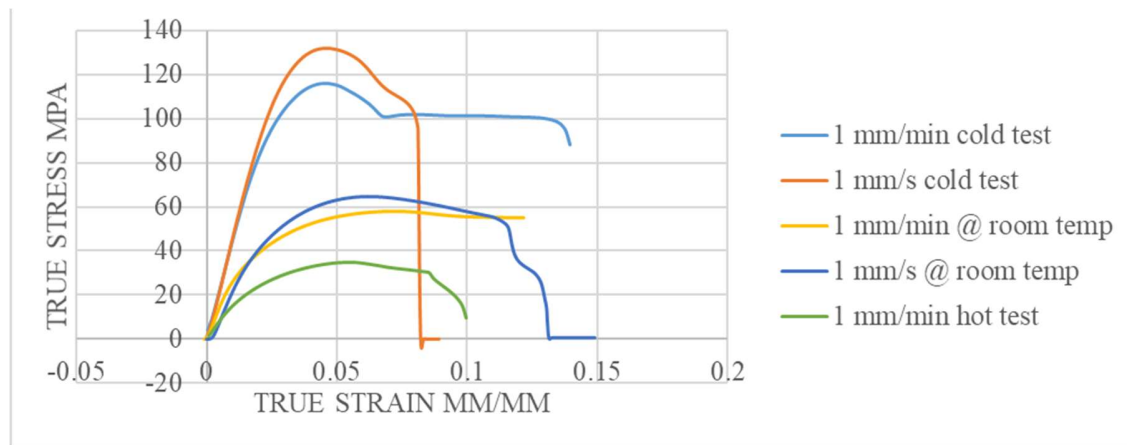


Fig. 12. True stress-strain curves for CB90 specimens.

Table 6. Quasi-static compression test on CB90 specimens.

Test number	Elastic modulus (Mpa)	Yield stress (Mpa)	Strain @ yield point (mm/mm)
CB90C #1 1 mm/min	4214	83	0.0217
CB90C #2 1 mm/min	4298	85.07	0.02179
CB90C #1 1 mm/s	4305	104	0.026

CB90R #1 1 mm/min	2721	29.6	0.0134
CB90R #2 1 mm/min	2658	32.52	0.0182
CB90R #1 1 mm/s	2818	34.6	0.014062
CB90H #1 1 mm/min	1655	15	0.01132
CB90H #2 1 mm/min	1551	17	0.01342

3.2.2 Compression test results for CB00: Test on black material (Fibremod™ GB335SFB), specimens are parallel to the sleeper's centerline

Table 7 and Fig. 13 present the compressive behavior of CB00 specimens under different testing conditions. The effect of temperature is more significant than the effect of loading rate on the mechanical behavior of CB00 specimens.

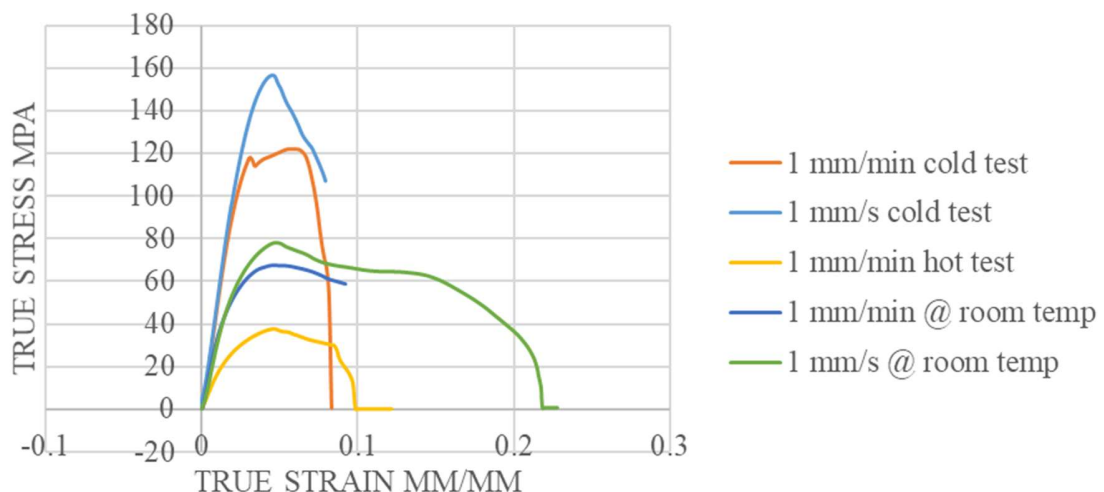


Fig. 13. True stress-strain curves for CB00 specimens.

Table 7. Quasi-static compression test of CB00 specimens.

Test number	Elastic modulus (Mpa)	Yield stress (Mpa)	Strain @ yield point (mm/mm)
CB00C #1 1 mm/min	4495	103	0.033
CB00C #1 1 mm/s	4539	123	0.029
CB00H #1 1 mm/min	1794	23	0.014
CB00H #2 1 mm/min	1727	19.92	0.01356
CB00R #1	3505	40.5	0.01355

1 mm/min			
CB00R #2	3346	38.92	0.013628
1 mm/min			
CB00R #1	3470	38	0.013046
1 mm/s			

3.2.3 Compression test results for CW specimens; White material (GD5150K)

The true stress-strain curves for CW specimens under compressive load are presented in Fig. 14. Elastic modulus, yield point stress are listed in Table 8 for each testing condition.

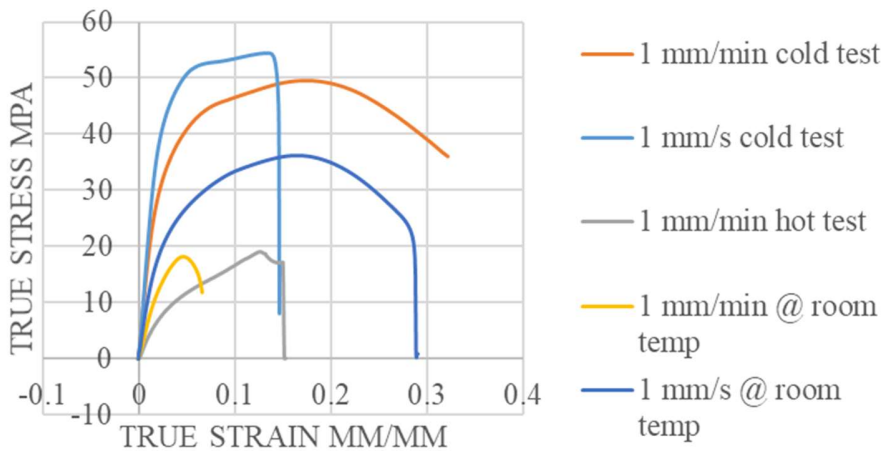


Fig. 14. True stress-strain curve for CW specimens.

Table 8. Quasi-static compression test of CW specimens.

Test number	Elastic modulus (Mpa)	Yield stress (Mpa)	Strain @ yield point (mm/mm)
CWC #1 1 mm/min	1801	23.62	0.01511
CWC #1 1 mm/s	2156	33.5	0.0174
CWH #1 1 mm/min	420	6.3	0.01700
CWH #2 1 mm/min	460	6.04	0.0151
CWR #1 1 mm/min	630	11	0.020
CWR #2 1 mm/min	669	9.98	0.0167
CWR #1 1 mm/s	1183	13.5	0.0134

3.3 Post compression inspection

Generally, both black material (CB specimens) and white material (CW specimens) underwent buckling after critical compressive load, as depicted in Fig. 15. Thus, elastic modulus, yield stress (strain @ yield point), and maximum stress are reported in this report⁶. This buckling behavior had been observed for all CW specimens under 1 mm/min and 1 mm/s and at three different temperatures (room temperature, cold temperature, and hot temperature). However, for CB specimens (black material) loading rate and temperature caused changes in the fracture morphologies.

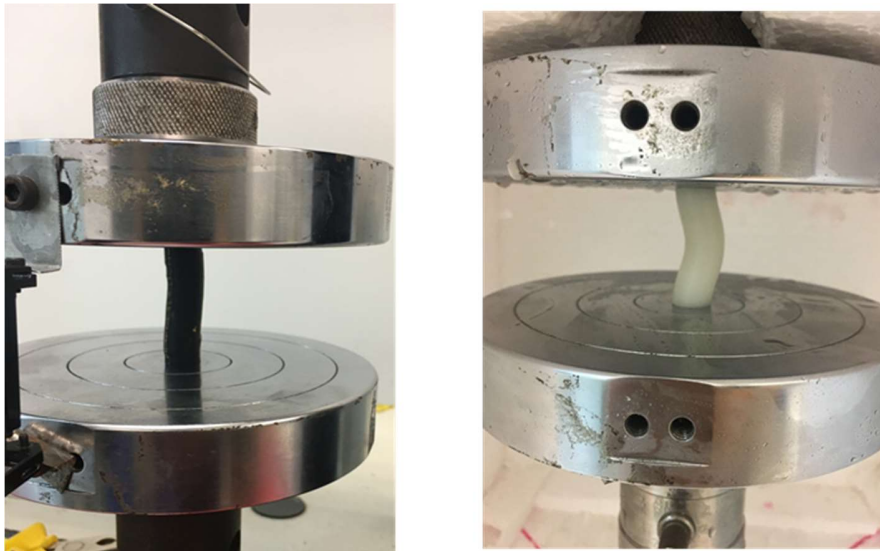


Fig. 15. Buckling of specimens under compressive load.

For hot tests, all CB specimens (black material) underwent global buckling (although initial failure with 45° sliding occurred before global buckling) similar to the failure mechanism that is illustrated for CB00R- 1 mm/min in Fig. 16. However, for low temperature (~30°C) and/or higher velocity (1 mm/s) tests, post-failure buckling had not been observed, see Fig. 16 for CB00C-1mm/min and CB00R-1mm/s.

⁶ For compressive strength, shorter cylindrical specimens may be required to alleviate the buckling problem.

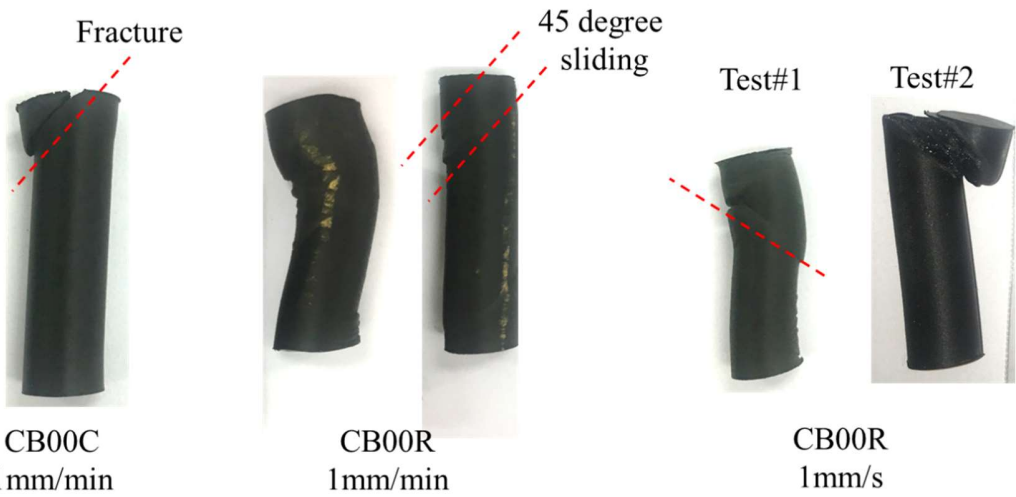


Fig 16. Effect of loading rate and temperature on the failure of black specimens under compressive load.

4. Split Hopkinson Pressure Bar (SHPB) test

Specimens (disks having 5 mm thickness and 15 mm diameter shown in Fig. 17) were cut from the components. For black material (GB335SFB) two sets of samples were cut from the sleeper with orthogonal orientations that are explained in Fig. 4. Fig. 18 shows the SHPB testing system and some equipment.



Fig. 17. Specimens for SHPB test.

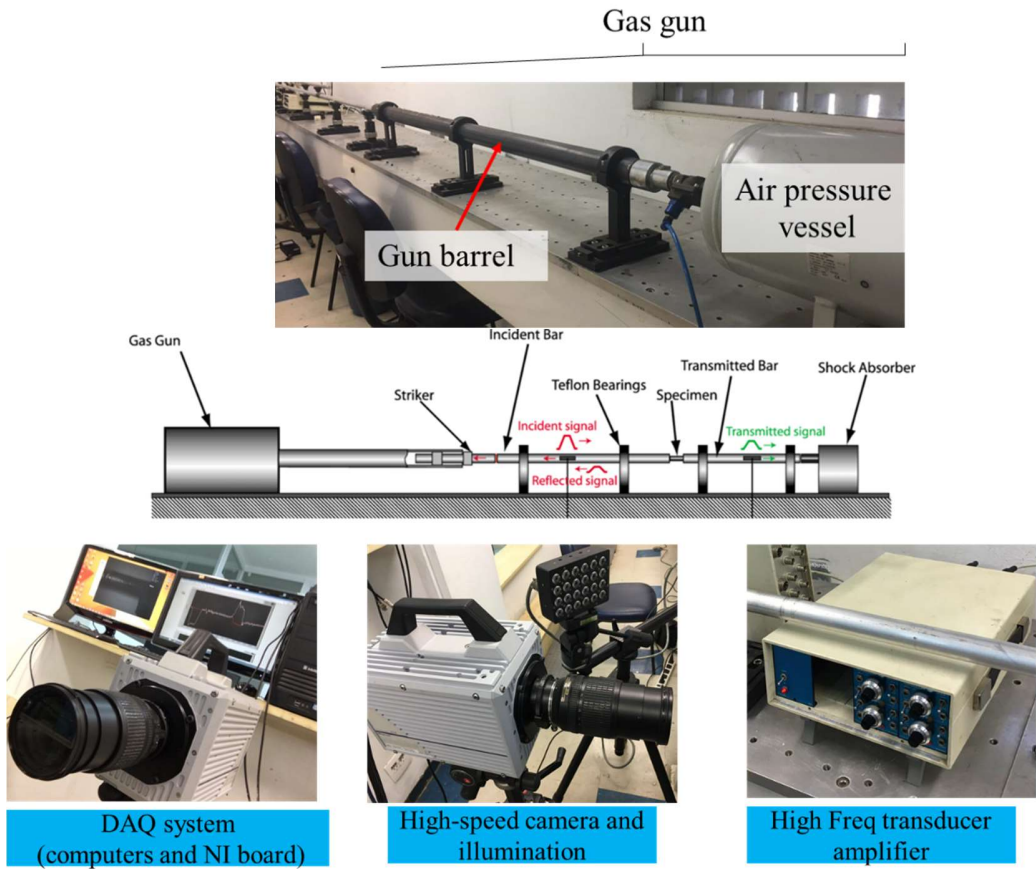


Fig. 18. SHPB and equipment.

4.1 SHPB test conditions

Since the duration of the tests is in order of a fraction of a second, heat transfer during tests is negligible. Thus, all tests (room temperature, cold test, and hot test) were conducted without considering the thermal chamber during tests. Specimens for cold (hot) tests were placed in the cold (hot) chamber for one hour to ensure a uniform temperature in the specimens. Then each specimen was removed from the chamber and put between SHPB bars, and the test was done in less than 15 seconds.

4.2 SHPB results

Rate sensitivity of materials is illustrated in Fig. 19 to 27 by comparing true stress-strain curves (add text).

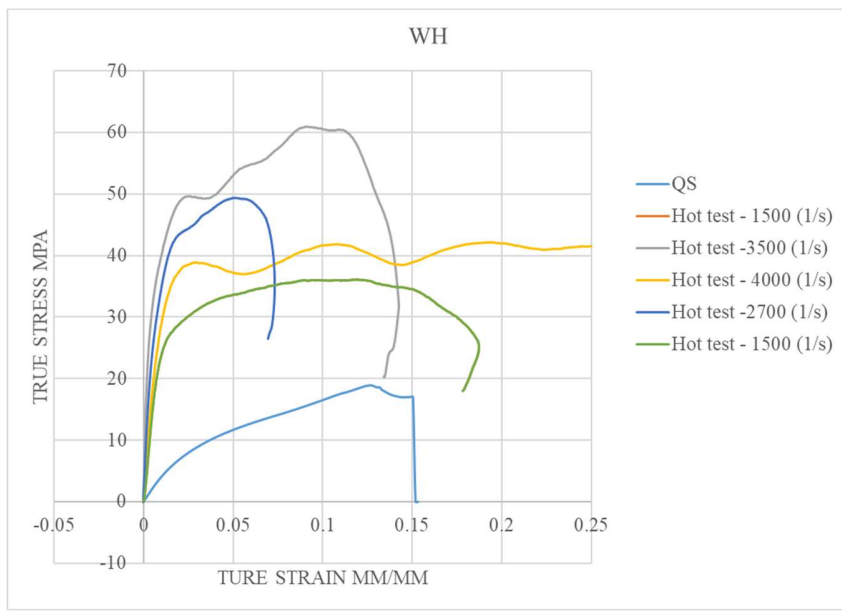


Fig 19. True stress-strain curves of hot test of white material.

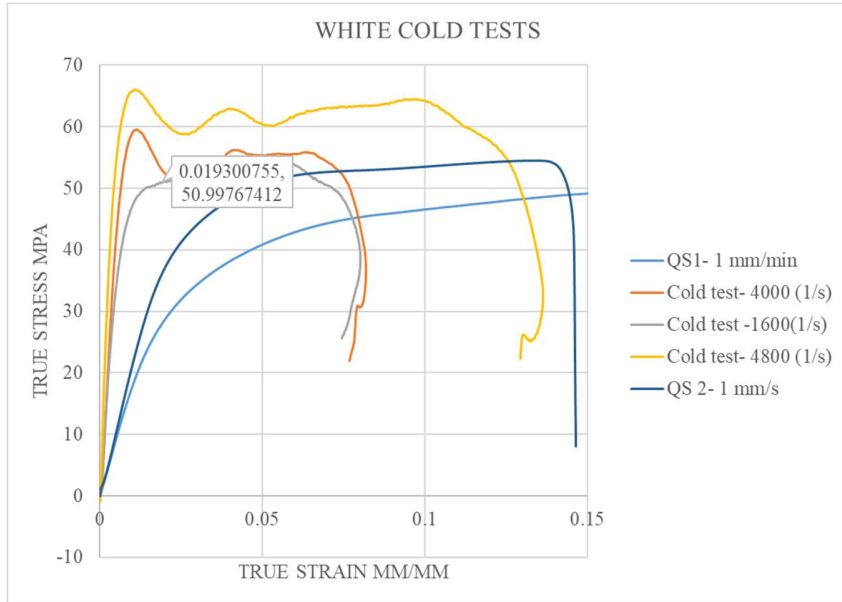


Fig 20. True stress-strain curves of cold test of white material.

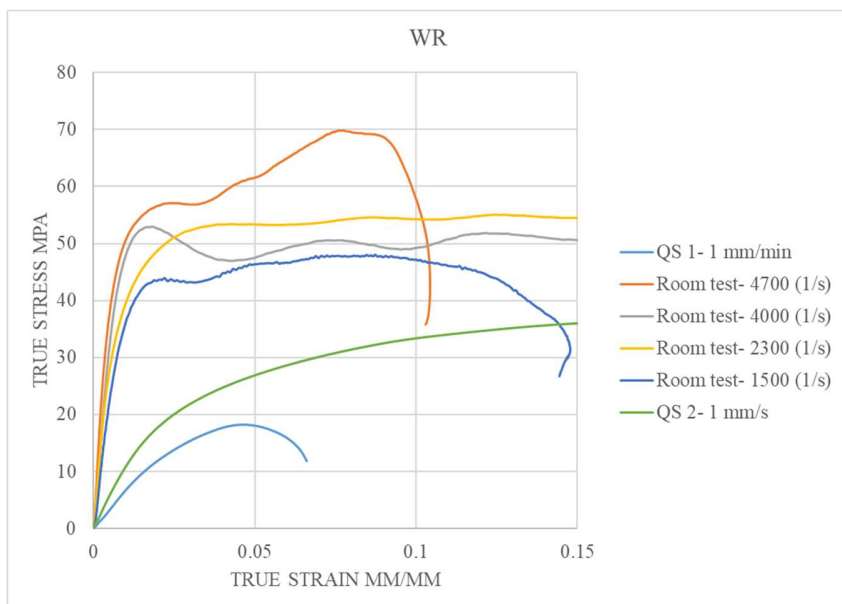


Fig 21. True stress-strain curves of room temperature test of white material.

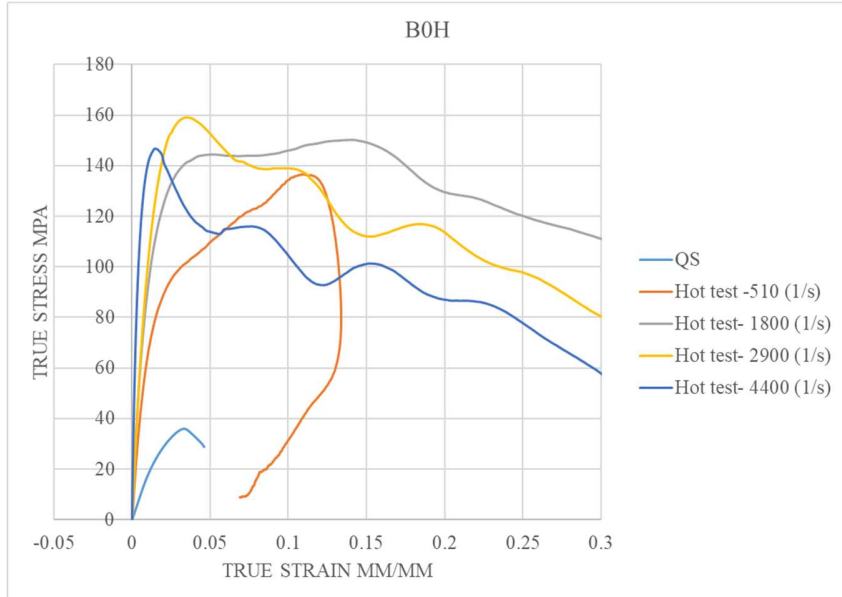


Fig 22. True stress-strain curves of hot test of black material samples were cut in a 0-degree direction.

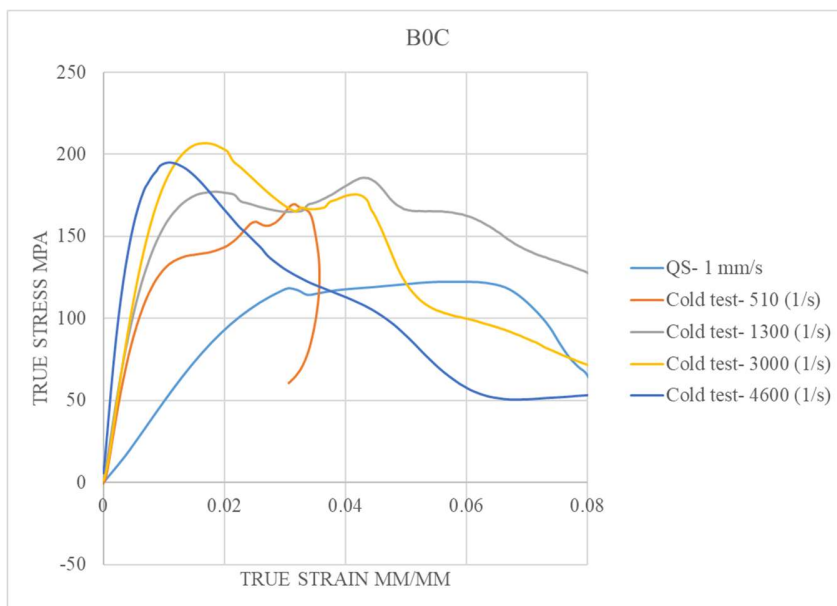


Fig 23. True stress-strain curves of cold test of black material samples were cut in a 0-degree direction.

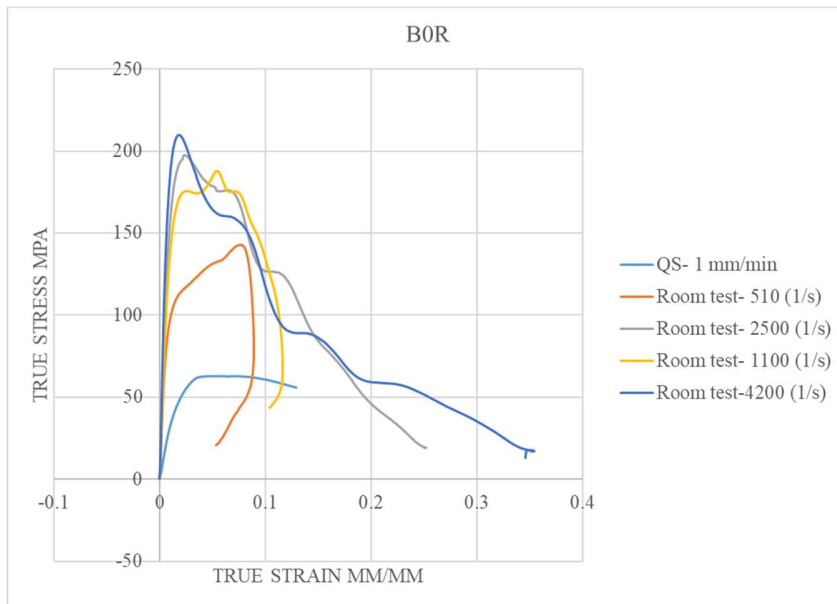


Fig 24. True stress-strain curves of room temperature test of black material samples were cut in a 0-degree direction.

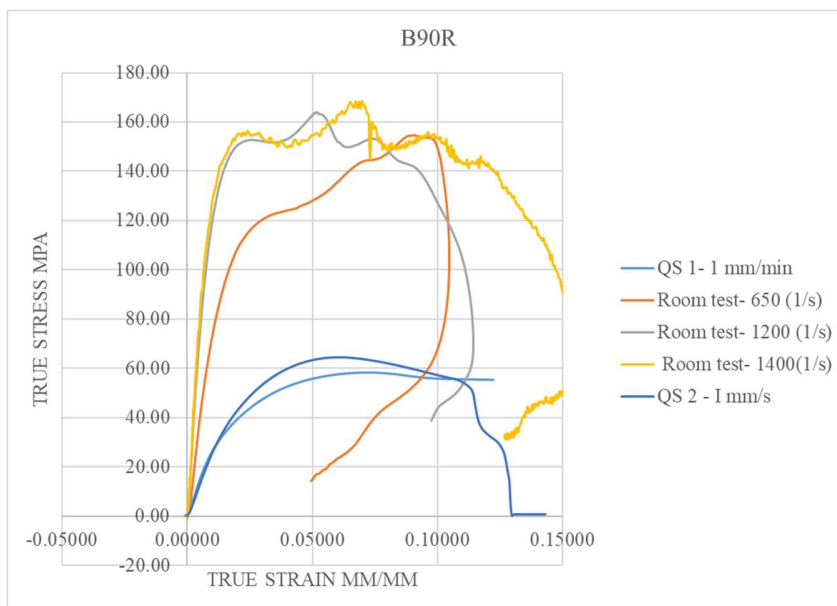


Fig 25. True stress-strain curves of room temperature test of black material samples were cut in a 90-degree direction.

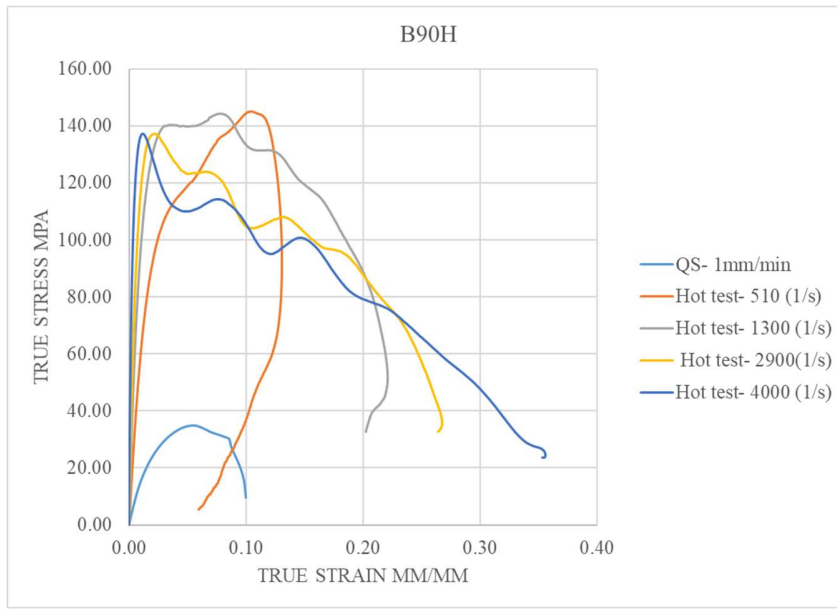


Fig 26. True stress-strain curves of hot test of black material samples were cut in a 90-degree direction.

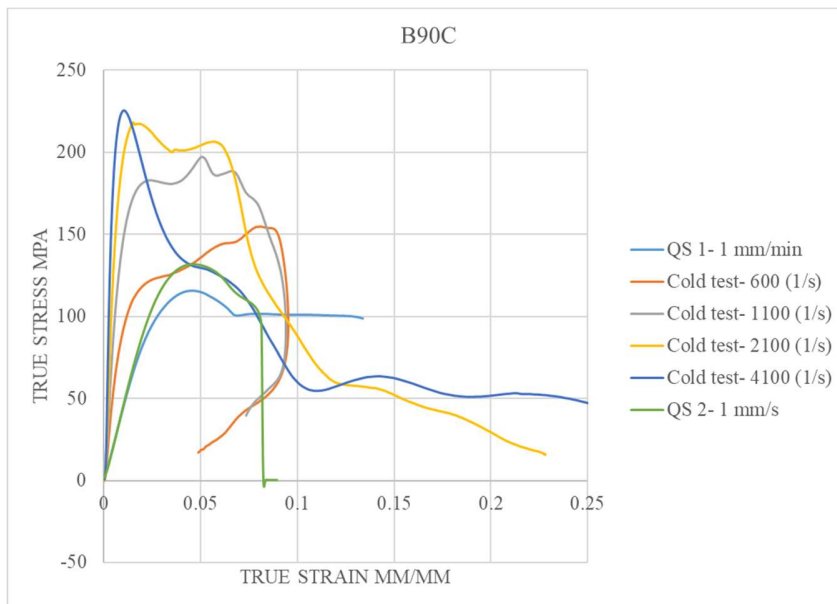


Fig 27. True stress-strain curves of cold test of black material samples were cut in a 90-degree direction.

Publications

Finite element modeling of crushing of CFRP cylindrical tubes under low-velocity axial impact



Composite Structures

Volume 280, 15 January 2022, 114902



Finite element modeling of crushing of CFRP cylindrical tubes under low-velocity axial impact

P.B. Ataabadi ^a, D. Karagiozova ^b, M. Alves ^a

Show more ▾

Submitted paper to Mecsol 2022

Partial results of material characterization of polymeric composite has been submitted as a paper to Mecsol 2022 conference.

Paper

ID
MECSOL2022-0076

Title
Impact response of polymeric train sleepers

Submission Author
pouria Bahrami Ataabadi

Paying Author
pouria Bahrami Ataabadi

Area
Impact Engineering

Step
Abstract

Status
Accepted

Presenter
pouria Bahrami Ataabadi

Presentation type
Poster

Authors - in the same order as they appear in the paper
pouria Bahrami Ataabadi
RENATO VARGAS
Marcilio Alves